R76-922241-4

12
NW

BROADBAND AND HIGH POWER INFRARED WAVEGUIDE MODULATORS

FINAL TECHNICAL REPORT

PERIOD COVERED
25 AUGUST 1972 TO 15 OCTOBER 1976

CONTRACT NO. N00014-73-C-0087

SPONSORED BY
ADVANCED RESEARCH PROJECTS AGENCY
ARPA ORDER NO. 1860, AMENDMENT NO.6

UNITED TECHNOLOGIES RESEARCH CENTER
EAST HARTFORD, CONNECTICUT 06108

DISCLAIMER NOTICE

THIS DOCUMENT IS THE BEST QUALITY AVAILABLE.

COPY FURNISHED CONTAINED A SIGNIFICANT NUMBER OF PAGES WHICH DO NOT REPRODUCE LEGIBLY.

UNITED TECHNOLOGIES RESEARCH CENTER

UNITED TECHNOLOGIES

East Hartford, Connecticut 06108

(14) UTRC/R76-922241-4

(9) Final Technical Report. 25 Aug 72 - 15 Oct 76

(6) Broadband and High Power Infrared Waveguide Modulators

By

(10) P. K. Cheo, M. Gilden, and R. Wagner
United Technologies Research Center
East Hartford, Connecticut 06108

October 15, 1976 (11) 15 Oct 76

Principal Investigator - P. K. Cheo (203) 565-4297

(12) 49 p.

Prepared for the Office of Naval Research
Contracting Officer: Dr. M. White
(15) Contract No. N00014-73-C-0087, new
Contractor Modification No. P00003 - $438,488
25 August 1972 to 15 October 1976

Sponsored by: ARPA Order-1860

Advanced Research Projects Agency
ARPA Order 1860, Amendment No. 6

409252 HB

Broadband and High Power Infrared Waveguide Modulators

TABLE OF CONTENTS

LIST OF FIGURES

LIST OF FIGURES (Cont'd)

R76-922241-4

Broadband and High Power Infrared Waveguide Modulators

1.0 SUMMARY

The objective of this program is to develop an efficient and reliable ultra-wideband waveguide modulator for CO_2 lasers that will be useful for high resolution imaging optical radars and high-data-rate optical communication systems. Efficiency and reliability can be obtained by using integrated optics technology, which is an optical analog of IC technology in electronics. The major advantage of this approach is derived primarily from the fact that strong and wideband interaction between the laser and the microwave electric field can be obtained within a thin waveguiding layer at a thickness of approximately one optical wavelength. However, the practicality and applicability of this approach remained to be proven. Of most importance is the ability to demonstrate that the ultimate performance of an integrated-optic modulator can supersede that of the conventional bulk modulators.

Since integrated optics is a new technology, it was recognized early in this program that the development of an efficient and reliable infrared waveguide moderator was dependent on a number of "breakthroughs". Therefore, this program was organized into several phases of investigation, that were carried out over a period of four years. The first year involved the investigation (Refs. 1,2) of various modulation techniques which can be performed by using thin-film waveguide modulators and the establishment of a figure of merit among various modulation techniques. The second year was devoted to demonstrating (Refs. 3,4) microwave modulation of CO_2 lasers in a thin-slab GaAs waveguide. The third year effort was concerned with advancing (Refs. 5,6) the waveguide modulator structure so as to have the required mechanical strength, high power handling capability, and nearly perfect optical transmission characteristics. The fourth year was devoted to achieving (Ref. 7) the highest sideband power from a CO_2 laser and the broadest modulation bandwidth at microwave frequencies.

During the past two year period (Summer 1974 to Summer 1976), this program has experienced an extraordinary growth. The progress can be measured

simply by the enormous increase in our ability to generate the sideband power at microwave frequencies. Table I summarizes the progress on the waveguide modulator performance.

TABLE I. PROGRESS SUMMARY

	1974	1975	1976
Sideband Power (mW)	<0.05	40	200
Modulation Bandwidth (GHz)	0.3	1.0	>8.0*

*Not as flat as predicted by theory

Results of Table I indicate that an improvement in sideband power delivery by a factor of 4,000 has been obtained during the past two year period. This remarkable achievement is attributed mainly to our persistent effort in advancing our waveguide fabrication techniques. By investigating various structural configurations, we found that for high power and broadband applications, two-dimensional tapered ridge waveguides, which are fabricated by the ion-beams milling technique and bonded on copper substrates, are found to be the best choice. With a 15 W CO_2 laser of a beam size $\leq$ 1 mm in diameter, 78 percent power coupling in and out of a tapered waveguide has been obtained while keeping the electrodes loss to a minimum value of 0.05 cm^{-1}. Broadband modulation of a CO_2 laser has been achieved with these devices at a bandwidth which exceeds several gigahertz. The sideband power conversion efficiency was measured to be 2.1 percent for the input microwave power of 60 W at 16 GHz. These bonded-down GaAs thin-slab modulators on copper substrates, with typical dimensions of 1 mm wide channel and 2.8 cm interaction length and 25 μm thick, are capable of delivering microwave modulated infrared laser power exceeding 200 mW with good transmitted beam quality.

2.0 INTRODUCTION

Electrooptic interaction in bulk crystals, whose refractive indices can be varied upon application of intense electric field, usually requires large amounts of electric power. This modulation power increases rapidly with increasing laser wavelength, λ, and, as a rule, follows a λ^3 functional relationship. Therefore, it is extremely difficult to generate electrooptic effect at infrared wavelengths. To overcome this difficulty, we have explored the use of thin-film waveguide devices, which are fabricated by using either epitaxially grown thin films (Refs. 8,9) or mechanically polished (Ref. 10) and ion-beam milled (Refs. 11,12) thin slabs. This report presents only the infrared waveguide structures that are suitable for high power laser system applications. Of particular interest is the performance of broadband modulation for a high power CO_2 laser beam. This modulator has potential applications in optical imaging radar, high-data-rate communications and in high-resolution spectroscopy where a narrow line width tunable over several gigahertz bandwidth is needed. The best design approach for these applications is to generate a single sideband power from a CO_2 laser carrier at microwave frequencies. In this case, broadband modulation can be obtained by sweeping the microwave frequency over a range of several gigahertz. This design was first demonstrated (Ref. 3) by interfacing a high power infrared waveguide with a microwave ridge transmission line. In order to minimize the propagation loss of the modulation field at microwave frequencies, the electrodes must be made of copper and must be in direct contact with the waveguiding layer. This requirement rules out the use of epitaxial waveguide structures (Ref. 13) and hence necessitates the use of a thin dielectric slab waveguide configuration. The top electrode must be in the form of a very long and narrow strip in order to provide the desired sideband conversion efficiency. The use of a microstrip electrode can produce significant distortion of the output laser beam shape by spreading and deflecting the beam in the plane of the waveguide. This beam distortion can be eliminated by using a wider electrode such that, along the entire propagating path, laser power is confined within the electrode width. However, widening of the electrode is not desirable because it reduces both the conversion efficiency and the modulation bandwidth. An alternative technique for confining the laser beam within a narrow and long propagation path is to use channel waveguides which can be made by removing small amounts of material along the edges of the microstrip electrode. With this technique we have obtained nearly perfect alignment of the optical beam with the microwave field along a narrow (1 mm wide) microstrip electrode over a propagation length of 4 cm. Furthermore, the transmitted laser beam quality is not degraded from that of the incident beam.

The most efficient coupler for an infrared laser beam to get in and out of an optical waveguide is the right-angle prism (Ref. 14). By using two germanium prisms at thinned coupling ports, we have obtained a transmitted laser power of 10 W through a 3 cm long metal-cladded GaAs thin-slab waveguide. The coupling efficiency, in this case, is 78 percent for the input coupler and 100 percent for the output coupler. Waveguides used in this work have been specially designed to accommodate the use of prisms as couplers. For high power application, the GaAs thin-slab waveguide must be bonded on a copper substrate, which not only provides the necessary structural strength to permit the use of prism couplers, but also improves the power-handling capability. With proper bonding and heat-sinking techniques, we have demonstrated that these GaAs thin-slab waveguides (25 μm thick) can be operated at a combined optical and microwave power level of up to 100 W.

Microwave losses in the microstrip transmission line and input matching into the thin-slab GaAs waveguide have been investigated (Refs. 3,4,6,7) in detail. By using copper electrodes at thickness greater than 10 μm, the measured microwave loss in the line is approximately 0.7 dB/cm. Nearly perfect matching has been achieved at resonant frequencies of the line by using only a one-step input transformer, located at the center of the microstrip electrode. With this network the measured full width of the sideband power is typically 1 GHz, and the sideband power conversion efficiency is found to increase linearly with increasing microwave input power. At an input of 60 W, the measured conversion efficiency is 2.1 percent. Broader impedance matching could be obtained by using two- or three-step transformers. Analysis indicates that, in the case of a three-step transformer, a relative flat-frequency response can be obtained in the range from 12 to 20 GHz.

3.0 HIGH-POWER IR WAVEGUIDE MODULATOR DEVELOPMENT

3.1 Introduction

During the past five years, United Technologies Research Center has engaged in an exploratory research and development program directed toward the investigation of the performance of infrared waveguide modulators under a work order from DARPA. This DARPA program was directed toward advancing the state of the art of this device for the generation of highest sideband conversion efficiency at microwave frequencies with particular emphasis at 16 GHz with a 1 GHz bandwidth. The high efficiency of the device is obtained by using integrated optics technology to confine the optical and microwave power in a small interaction region in the form of a thick-film medium at a thickness of about 25 μm. A factor of 10^2 enhancement in the field-induced birefringence and a factor of 10^4 in sideband power generation can be obtained by this approach as a result of reduction in thickness from the conventional bulk modulator configuration. In order to realize this advantage, an infrared waveguide modulator must be developed to the extent that it must transmit both the optical and the microwave power in an efficient manner. Under the DARPA program, we have produced infrared waveguide modulators that can transmit as much as 63.5% of the optical power and about 60% of the microwave power through an interaction path length of 3 cm. These results are very close to the theoretical limits for perfect waveguides. The difference in power transmission between the waveguides and bulk devices is almost insignificant in view of the enormous gain in modulation performance.

The waveguide modulator developed under this program not only has demonstrated its efficiency but also has proven its power-handling capability. Several waveguide modulators have been tested with intense optical and microwave fields. With a focused CO_2 laser beam at 15 W, which corresponds to a power density of 80 kW/cm^2, and a microwave power input of 60 W, a single sideband power of 0.2 W has been generated at frequencies in the neighborhood of 16 GHz off-set from any one of the vibrational-rotational CO_2 laser lines.

Since the sideband power increases linearly with an increase in both the optical and the microwave power and almost quadratically with an increase in the interaction length, a great emphasis has been placed on the fabrication of extraordinarily long GaAs electrooptic waveguides which are suitable for high-power applications. To strive for perfection, submicron tolerances in the fabrication of long optical and microwave circuits must be maintained. In this section, the optical waveguide structures and their transmission characteristics will be presented and fabrication and processing techniques will be summarized. Microwave modulation of the CO_2 laser and the waveguide modulator performance and characteristics will also be detailed.

3.2 Infrared Electrooptic Waveguides

Either epitaxially grown (Refs. 13, 15, 16) or mechanically polished (Ref. 17) infrared waveguides suitable for electrooptic modulation of laser radiation have been investigated only at very low optical power levels. As optical and/or electric input power and the modulation frequency are increased, device degradation from electrical power loss at high frequencies, surface deformation by electrodes and stress-induced birefringence at the edges of electrodes and stress-induced birefringence at the edges of electrodes as well as waveguide imperfections and material defects become increasingly serious. We have explored several waveguide structures that may be suitable for high-power laser systems applications. Of particular interest is the device performance of a wideband electrooptic modulator for a high-power CO_2 laser beam. This modulator has potential applications in optical imaging radar, high-data-rate communications and in high-resolution spectroscopy where a narrow line width tunable over a bandwidth greater than several gigahertz is needed. The best design approach for these applications is to generate single sideband power from a CO_2 laser carrier at microwave frequencies. In this case, broadband modulation can be obtained by sweeping the microwave frequency over a range of several gigahertz. This design has been demonstrated (Ref. 11) by interfacing a high-power infrared waveguide with a microwave microstrip transmission line.

To minimize the propagation loss of the modulation field at microwave frequencies, the electrodes must be made of copper and must be in direct contact with the waveguiding layer. This requirement rules out the use of epitaxial waveguide structures and hence necessitates the use of a thin dielectric slab waveguide configuration. The top electrode must be in the form of a very long and narrow strip in order to provide the desired sideband conversion efficiency and the modulation bandwidth. Use of a microstrip electrode causes difficulty in beam alignment with respect to the strip line. We often observed that a slight misalignment of the laser beam can produce significant distortion of the output laser beam shape by spreading and deflecting the beam in the plane of the waveguide. This lens-like effect during the quiescent phase is caused by the waveguide surface deformation along the edges of the electrode, which produces a localized stress-induced birefringence that is typically one order of magnitude larger than the microwave field-induced birefringence at the power levels of interest. When microwave power is applied, beam distortion is enhanced as a result of thermal-induced birefringence. Beam distortion can be eliminated by using a wider electrode such that along the entire propagating path laser power is confined within the electrode width. In an experiment with a wider electrode, we observed no beam distortion either with or without the application of a microwave field. However, widening of the electrode is not desirable, because it reduces both the conversion efficiency and the modulation bandwidth. An alternative technique for confining the laser beam within a narrow and long propagation path, is to use channel waveguides which can be

made by removing small amounts of material along the edges of the microstrip electrode. With this technique we have obtained nearly perfect alignment of the optical beam with the microwave field along a narrow (1 mm wide) microstrip electrode over a propagation length of 3 cm. Furthermore, the transmitted laser beam quality is not degraded from that of the incident beam.

Previous studies (Refs. 5,7) indicated that optical transmission through the waveguides via prism couplers is typically about ten times that of grating couplers. This large difference in coupling efficiency is basically caused by two factors; the lower coupling strength of the grating and the partition of energy into multiple diffracted beams when the grating coupler is used. Furthermore, waveguide imperfections have much greater deleterious effects on the performance of grating couplers. For these reasons, the waveguide structure has been designed specifically to accommodate the use of prisms as couplers.

Broadband matching of microwave power into a GaAs thin-slab waveguide can be efficiently and reproducibly achieved if the top and the bottom copper electrodes have thicknesses $\geq$ 10 μm. In order to maintain the structural integrity of the waveguide, it is necessary to bond the metal-cladded thin-slab to a flat copper block. A bonded waveguide also provides the necessary structural strength to permit the use of prism couplers. Furthermore, use of the bonded-down structure improves the power-handling capability. With proper bonding and heat-sinking techniques, we have demonstrated that these GaAs thin-slab waveguides (25 μm thick) can be operated at a combined optical and microwave power level of up to 100 W.

Techniques have been developed to produce the bonded GaAs metal-cladded thin-slab waveguides with the specifications listed in Table II.

Table II Infrared Waveguide Specifications

Thickness	25 μm ± 1 μm (modulation region) 12 μm ± 1 μm (coupling region)
Length	> 4 cm
Channel Depth	$\gtrsim$ 5 μm
Surface Finish	Mirror like
Microstrip Electrode	1 mm x 2.8 cm (10 μm thick)
Bonding Layer	< 2 μm
Copper Substrate	Optical flat and parallel to 2 sec

A typical bonded GaAs thin slab waveguide is shown in Figure 1. The structure is resting on two sliding wedges which are used to control the air-gap for prism couplers by pressing the top of the two prisms against a cover plate. The details of this bonded thin-slab waveguide modulator is shown in Figure 2. The optical polishing fixture with precision angular adjustments, as shown in this figure, is a very important tool during the initial stage of waveguide fabrication, which will be described in detail in Section 3.3. The thin-slab waveguide is made of high-resistivity ($> 10^8 \Omega$-cm) Cr-doped GaAs material and is cladded with 10 μm thick copper electrodes on both the top and the bottom surfaces. This metal-cladded thin-slab is bonded on an optically polished copper substrate by a 2 μm thick low viscosity epoxy.

Figure 3 is a plot of the waveguide thickness vs the modal index β/k for the TE modes of the thin-slab structure with a refractive index $n = 3.275$ at 10.6 μm. The refractive index of the media above and below the slab is taken to be unity. With metal-cladding, the absorption loss increases rapidly with decreasing waveguide thickness. Previous calculations (Ref. 13) indicated that a metal-cladded slab waveguide at a thickness of 25 μm has an attenuation coefficient of 0.055 cm^{-1} and 0.22 cm^{-1} for the TE_0 mode and TE_1 modes, respectively. At 15 μm, the attenuation coefficient increases to 0.25 cm^{-1} and 1.0 cm^{-1} for these modes. Also, the microwave loss increases rapidly with decreasing waveguide thickness. Therefore, use of long waveguide devices with thicknesses much below 25 μm leads to appreciable propagation losses.

Optical coupling depends critically on both phase and aperture matching (Ref. 14) of the laser beam with a guided-wave mode. At a phase-matched angle, the coupling efficiency η for a uniform input beam is given by (Ref. 14)

$$\eta = (2/\alpha\ell)\,(1 - e^{-\alpha\ell})^2 \qquad (1)$$

where ℓ is the input beam diameter, and α is the coupling parameter, which depends in a complicated way (Ref. 18) on the waveguide thickness, refractive index and gap-spacing δ between the prism base and the surface of the thin-slab. Using the formulations of Tien and Ulrich (Ref. 18), we found that η is a slowly varying function of δ and does not change more than 15% for δ values between zero and 0.1 μm. In practice, δ can easily be confined within this range. We have calculated the coupling efficiency of TE_0 and TE_1 modes for a laser beam size $\leq$ 1 mm. Results of this calculation are shown in Figure 4 as a function of the thin-slab waveguide thickness for δ = 0.1 μm and ℓ = 1 mm. For $\ell < 1$ mm, the peaks of these curves shift slightly toward smaller waveguide thickness values with very little change in their shapes. It is desirable to use small beam sizes because it is easier to obtain a broader modulation bandwidth with a narrower electrode. With a narrow electrode width, the characteristic impedance of the waveguide modulator can be raised to a value where a broadband

INFRARED WAVEGUIDE HOLDER ASSEMBLY

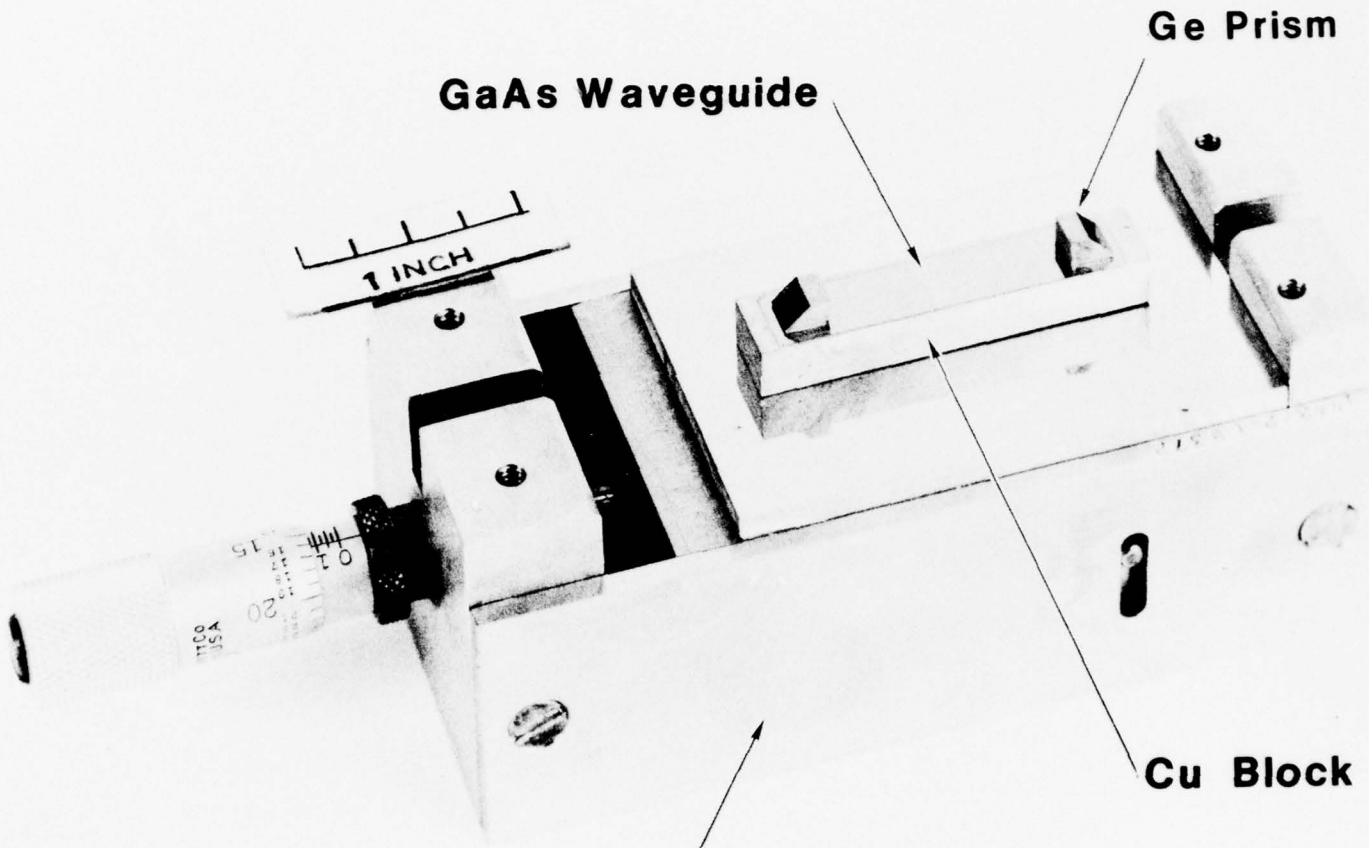

FIG. 1

UNITED TECHNOLOGIES RESEARCH CENTER

UNITED TECHNOLOGIES

BO9-176-3

TYPICAL HIGH-POWER IR WAVEGUIDE STRUCTURE

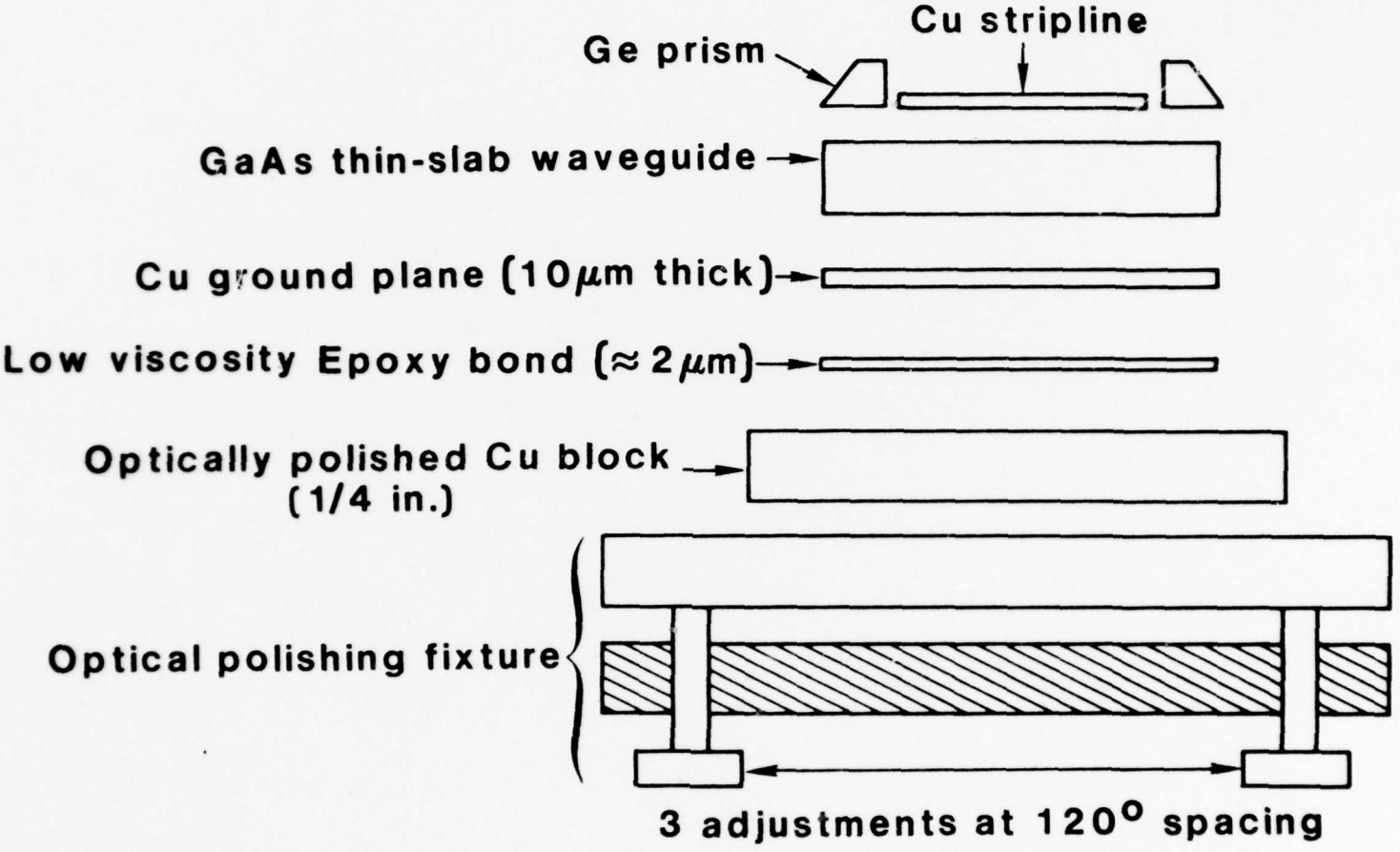

FIG. 2

WAVEGUIDE THICKNESS VS β/k

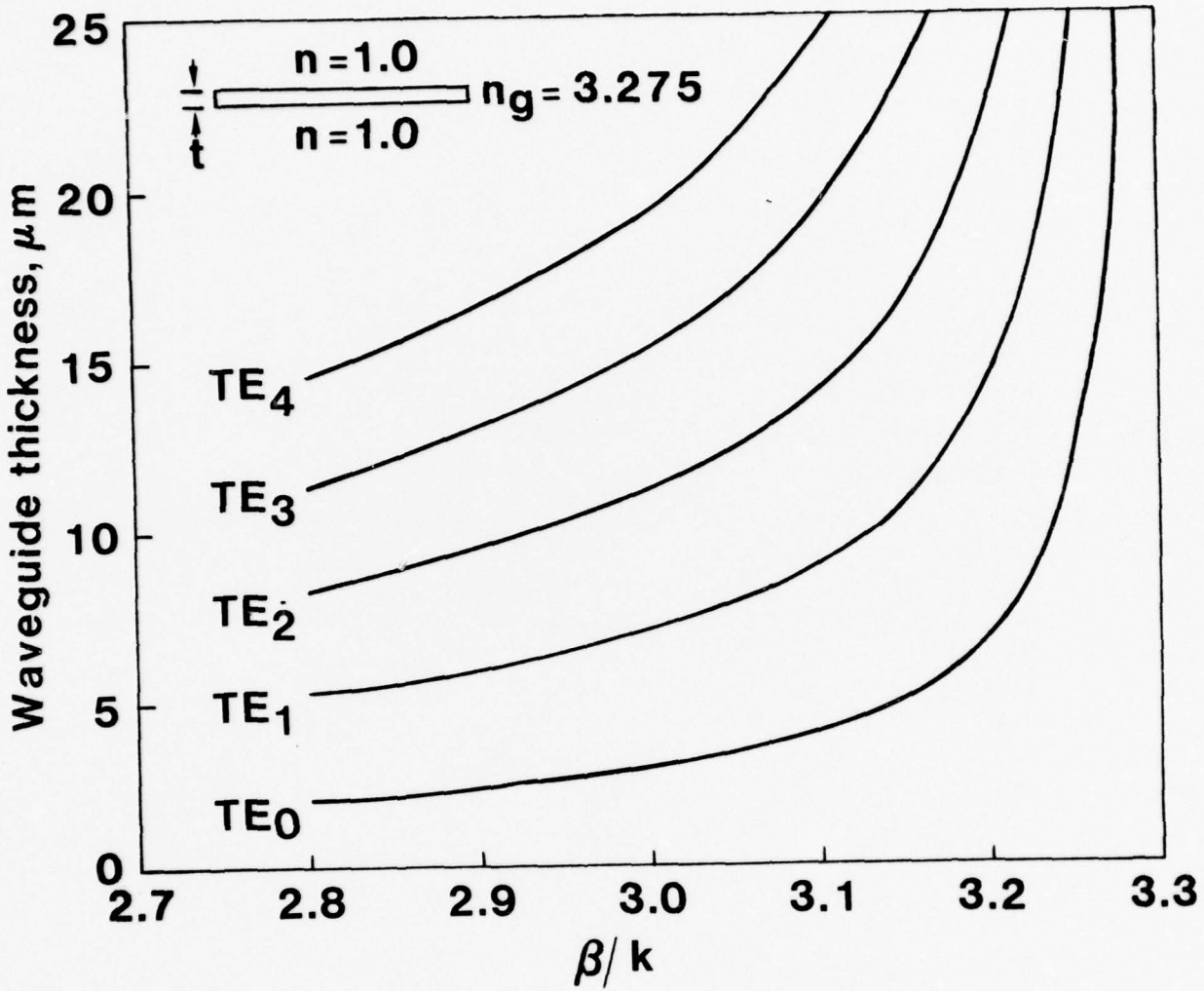

76-04-331 – 1

FIG. 3

UNITED TECHNOLOGIES RESEARCH CENTER

PRISM COUPLING EFFICIENCY VS WAVEGUIDE THICKNESS

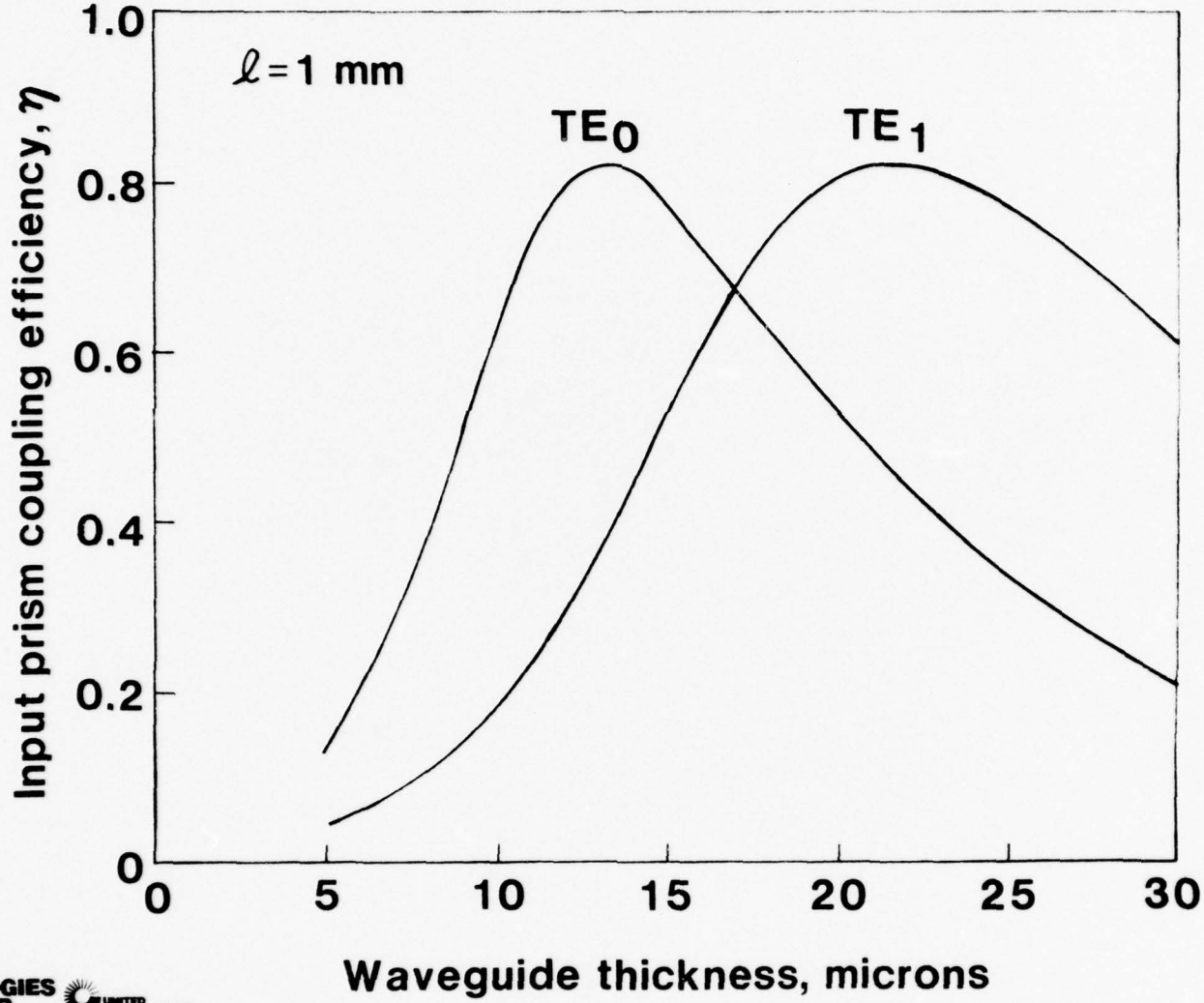

UNITED TECHNOLOGIES RESEARCH CENTER

FIG. 4

76-04-67-1

matching can be easily realized (Ref. 3). Results of Figure 4 indicate that for $t > 20$ μm, the most efficient coupling is obtainable for TE_1 modes, or the higher-order modes. To obtain efficient coupling of TE_0 modes, the thickness in the coupling region must be reduced to less than 15 μm. Most of our experimental studies, particularly on the electrooptic interaction, have been made with the planar waveguide structure. However, we have successfully fabricated several slowly tapered waveguides, as shown in Figure 5. Structural configuration of these tapered waveguides are similar to that of the planar waveguides except that the regions near the ends of the slab, where optical coupling occurs, is thinner than the central region. Typical thickness of the coupling region varies from 12 to 14 μm, and the thickness of the electrooptic interaction region is about twice that of the coupling region. The transition occurs gradually between the two regions over a length greater than 1 mm. In this way the modal character is not deteriorated to a significant extent. We have studied the optical transmission characteristics of these waveguides in detail, and have found that the optical power transmission through these tapered waveguides is greatly increased from that through planar waveguides as a result of the reduction in propagation losses.

The microstrip electrode on the waveguide surface always distorts the transmitted beam because of a stress-induced lens-like effect. To compensate the difference in refractive index at the edges of the electrode, we remove a small amount of GaAs material to form a simple channel waveguide, as shown in Figure 6a. For a 25 μm thick waveguide, a channel depth of 5 μm is more than sufficient to produce the desired beam confinement within a long and narrow propagation channel. To combine the features of both the channel and tapered waveguides, we have fabricated a slowly tapered raised-ridge waveguide, as shown in Figure 6b. The advantages of using such a type of structure are: (1) improved coupling efficiency for the TE_0 mode with small input beam sizes, (2) reduction of the propagation loss, (3) increase in the microwave driving power density by narrowing the ridge width, and most important, (4) elimination of the beam distortion caused by the top electrode in a stripe geometry. At a thickness of 25 μm, the power loss due to the absorption of the 2.8 cm long electrodes for the TE_0 mode is only about 13%. However, the waveguide thickness in the coupling region must be decreased to about 12 μm in order to excite the TE_0 mode efficiently.

3.3 Fabrication and Processing Techniques

All waveguides used in this work are made of high resistivity Cr-doped GaAs material which has been carefully selected and characterized from commercially available ingots of large size. These ingots are sliced into thin wafers at the

TAPERED WAVEGUIDE STRUCTURE

FIG. 5

CHANNEL WAVEGUIDES

a) Simple channel

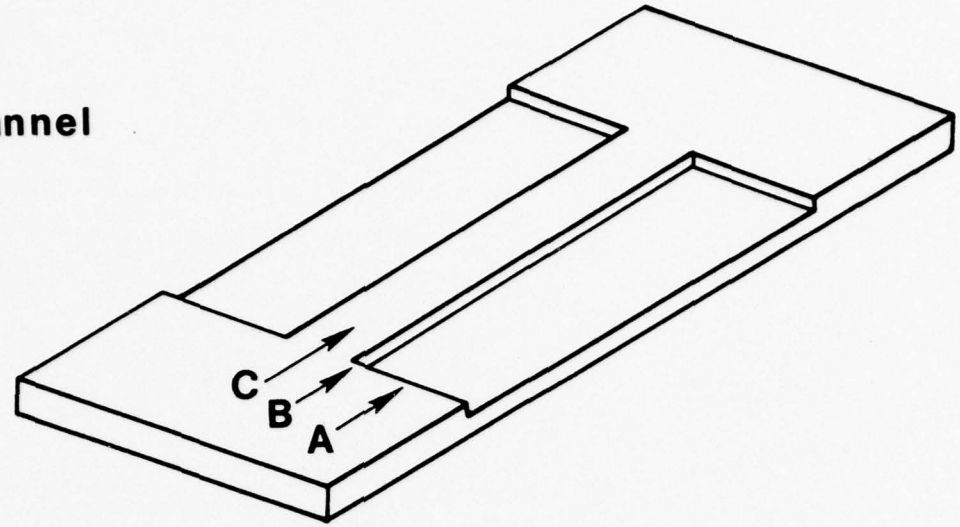

b) Slowly tapered, raise ridge channel

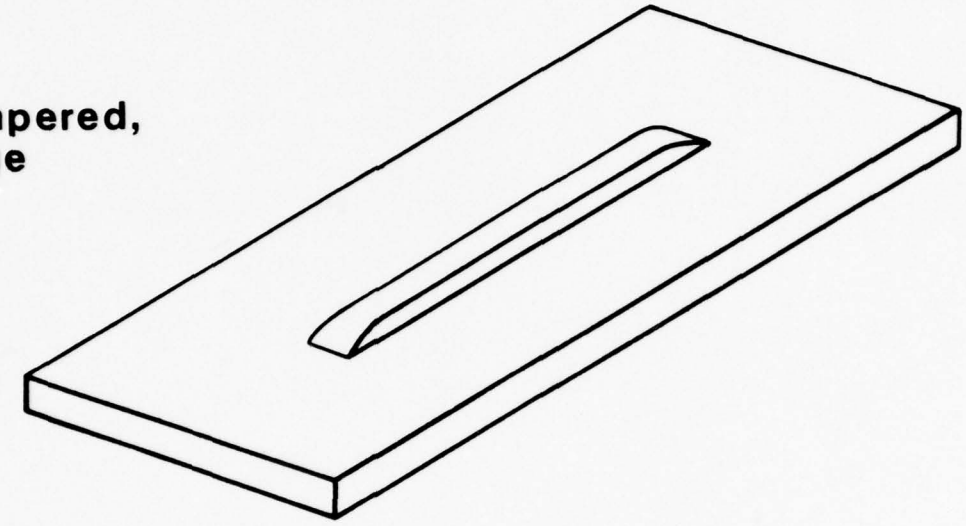

UNITED TECHNOLOGIES RESEARCH CENTER

76-02-196-1

FIG. 6

orientation (100) plane. The thickness of these saw-cut wafers is typically at 15 mils. The typical wafer size is large enough to yield 3 (1 cm x 4.5 cm) rectangular waveguides.

The first step in the fabrication procedure is to lap and polish one face of a 15-mil thick GaAs wafer to a thickness about 5 mils by using a precision polishing jig on a glass plate with 3 μm platelet alumina. The GaAs wafer is then chemo-mechanically polished by using a soft pad saturated with a solution of 100 ml distilled water to 6 ml of 6% sodium hypochlorite. A mirror-like finish is obtained when approximately 10 μm of GaAs is removed. At this stage the wafer is cleaved into a 4.5 cm x 1.0 cm waveguide configuration and is further thinned by a collimated beam of Ar^+ ions at a current density of 1.0 mA/cm^2 until 25 μm of material is removed. This thinning step is very important because it removes all mechanical process-induced damages to the material.

The ion-beam milled surface is electroplated with a 10 μm thick copper film, which forms the ground plane of the waveguide modulator. The wafer is then bonded to an optically polished copper block with a low viscosity resin (Stycast 1217). Typical thickness of a uniform bonding layer is about 2 μm, obtained by applying a uniformly distributed weight during the curing cycle. At this point the thickness of the GaAs wafer is about 8 mils. The waveguide is then lapped until approximately 2 mils of GaAs is removed. The surface is then chemo-mechanically polished to a mirror-like finish. During the processing, the thickness of the GaAs waveguide is measured at several points along the 4.5 cm length with a Perkin-Elmer Model 621 IR Spectrophotometer in the reflectance mode. The thickness variations determined by the IR spectrophotometer gives an indication of the wedging in the GaAs wafer only. With the above described thinned process, wedging is routinely found to be less than 2 μm along the 4.5 cm length of the 5 mil thick waveguide. The IR spectrophotometric measurements can also be compared with the measurements of the Hover-probe, which is a precision non-contacting air gauge instrument (Ames-Mercer). In general, very good agreement exists between these two independent measurements, which implies that the copper ground plane and bonding medium are essentially wedgefree. If any wedging does exist at this point it can be compensated by using the angular adjustments which are incorporated in the polishing fixture. At a 2.4 mil thickness, a chemo-mechanical polish is performed. Spectrophotometer scans are taken again of the GaAs thickness prior to the final ion beam thinning.

To improve the optical transmission characteristics, it is desirable to maintain the thickness of the interaction region thicker than that of the input and the output coupling region. The transition between the two regions should have a length not less than about 1 mm. To generate the required configuration, a shadow mask of aluminum oxide was made as shown in Figure 7a. Aluminum oxide was selected because of its slow ion milling rate. The shadow mask (2.77 cm long x 0.8 cm wide) is placed on top of a chemo-mechanically polished wafer. The

Mask for Ion-Milling of Tapered Waveguide

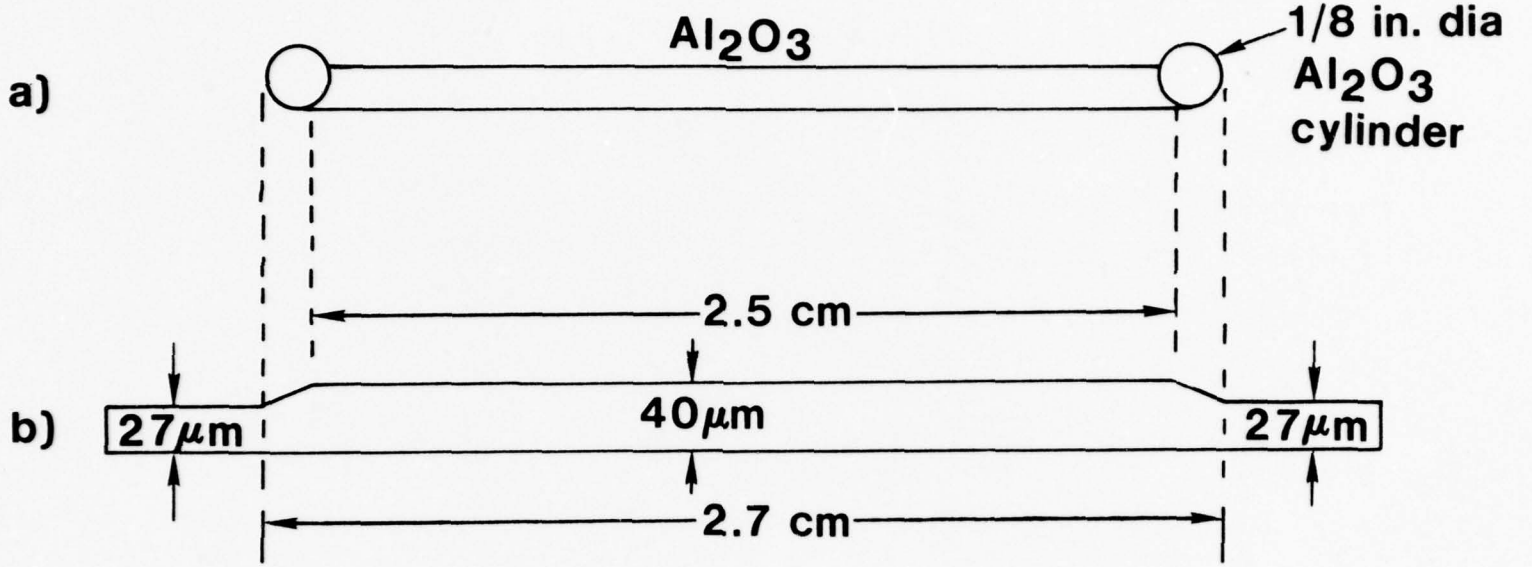

UNITED TECHNOLOGIES RESEARCH CENTER

76-04-318-1

FIG. 7

tapered step is formed by ion beam machining at a current density of 0.6 mA/cm^2 at normal beam incidence. The rate of GaAs removal is 6 μm/hr. The waveguide is machined until 13 μm of material is removed from the unmasked area. Figure 7b shows the resulting waveguide dimensions after performing the milling process. The wafer is further thinned by the ion-beam without the shadow mask until the desired thickness is obtained. In this process special precaution must be taken to maintain the substrate temperature below 50°C. It was found that the difference in thermal expansion between GaAs and the copper ground plane can cause cleavage in GaAs wafers if the temperature of the substrate is not controlled. A water cooling fixture was installed into the Vecco Microetch System. It was designed specially for the rotating holder to maintain a low temperature (< 50°C) under ion-bombardment over extended periods of time.

The fabrication of a microwave waveguide modulator is completed after a 10 μm thick copper film in the form of a microstrip electrode is applied to the top surface of the GaAs thin slab. This is accomplished by standard photolithographic and electroplating techniques. The two-dimensional channel or raised-ridge waveguide is produced by ion-milling a bonded GaAs waveguide modulator around the edges of the microstrip electrode.

3.4 Optical Transmission Characteristics

Optical transmission measurements were made with CO_2 lasers at power levels up to 15 W. For most experiments, the input laser power to the waveguides is in the range from 3 to 5 W in a focused beam spot of ≃ 1 mm in diameter. Results reported here were obtained by using two right-angle germanium prisms with a base area of 5 mm x 7 mm. A one-meter-radius reflecting mirror is used to focus the gaussian input beam to approximately 1 mm in size ($1/e^2$ laser power points at the input prism). Through the length of the waveguide the transverse beam configuration is essentially confocal, as shown in Figure 8. In the absence of the top electrode, a beam that is nearly identical to that of the input beam can be obtained in the far-field of the output prism for waveguides having a thickness uniformity better than ± 5%. When a top microstrip electrode (1 mm wide x 2.8 cm long) is deposited on the surface of a bonded thin-slab GaAs waveguide, the transmitted laser beam shape is severely distorted, as shown in Figure 8, for an incident beam size of ≥ 0.7 mm propagating underneath the electrode. However, the out-coupled angle does not appear to be affected. The output beam quality is restored if the propagation path is outside the electrode region. The elliptical output becomes asymmetric if the confocal beam is slightly misaligned with respect to the electrode. The elliptical distortion increases further with applied microwave power. We attribute the cause of the above observed lens-like effect to a stress-induced birefringence along the edge of the electrode. Because of the electrode geometry, it is very difficult to achieve a perfect alignment.

EFFECT OF ELECTRODE ON A GUIDED MODE

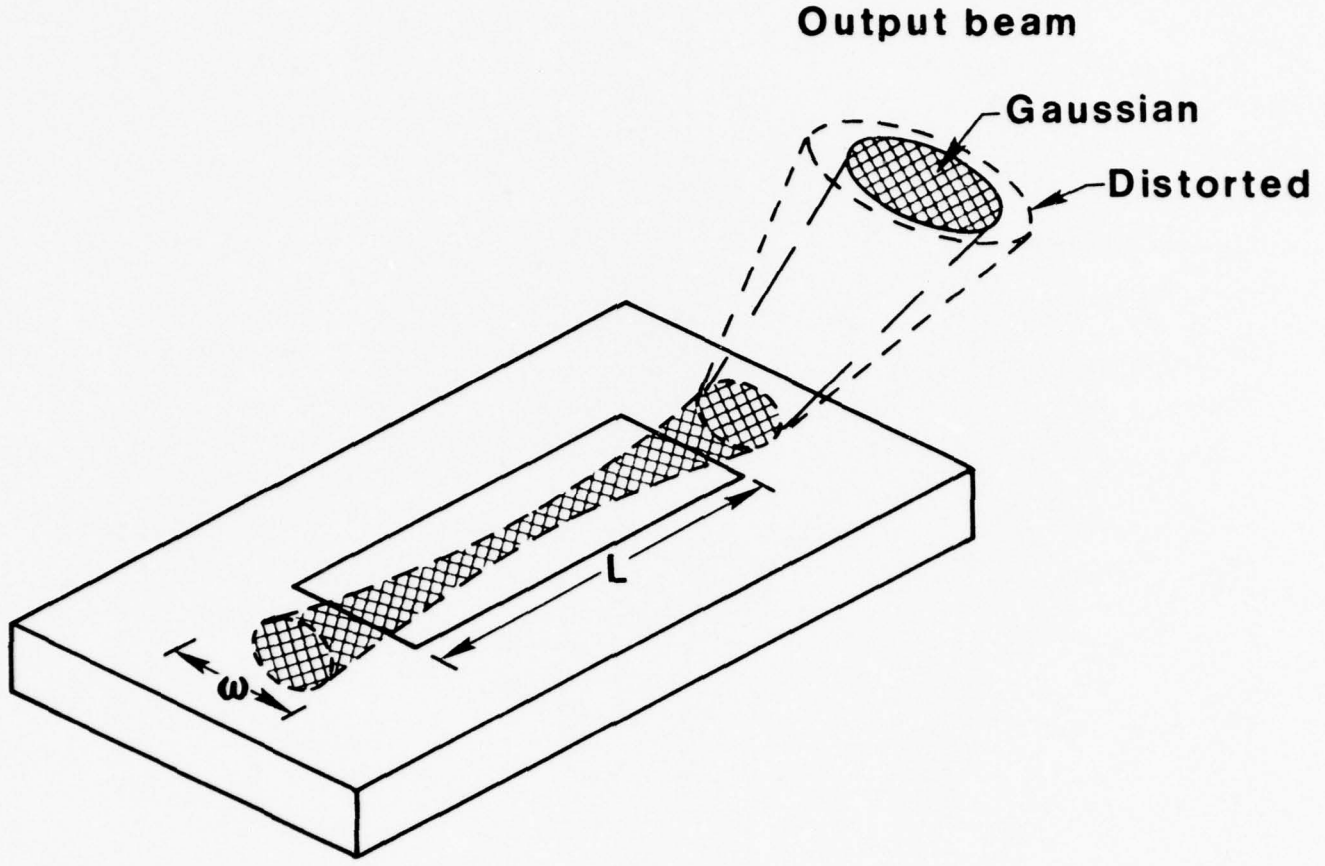

UNITED TECHNOLOGIES RESEARCH CENTER

76-02-196-2

FIG. 8

A diffraction-limited beam can only be collimated within the narrow microstrip with its width to length ratio, w/L, as given by (Ref. 19)

$$w^2/L \geq 9(4\lambda/n\pi) \tag{2}$$

where λ and n are the laser wavelength and refractive index, respectively. For a width of 1 mm, the length in accordance with Eq. (2) cannot exceed 3 cm.

Experimentally we found that this lens-like effect can be eliminated by increasing the electrode width from 1 mm to 2 mm for an input beam size of 1 mm. From the modulator design point of view this increase is not desirable because an increase in electrode area causes both an increase in the device capacitance (or a decrease in characteristic impedance) and a reduction in the modulation bandwidth and power density. A more desirable approach is to compensate the difference in refractive index at the edges of the electrode by removing a small amount of GaAs material to form a simple channel waveguide, as shown in Figure 6a. With such a waveguide, we have confined the beam to a 1 mm channel path in the presence of a microstrip electrode. The transmitted laser beam shapes through a channel waveguide with a channel dept of ~ 5 μm are shown in Figure 9. Figure 9a depicts the input beam shape; Figure 9b shows the output beam shape when a TE_1 mode is launched from point A as indicated in Figure 6a. Two finite steps in the waveguide do not cause discernable beam distortion but only cause a slight decrease in the transmitted power as compared with that transmitted through the channel. Figure 9c shows the output beam shape when a TE_1 mode is launched from point C, as indicated in Figure 6a, which is located in the center of the channel with its top surface coated with a 10 μm thick copper film. In this case, the spread of the out-coupled beam is diffraction-limited by the width of the channel but is not affected by the microwave power. If the laser is incident at point B, which is located at the edge of the channel, the output splits into two beams as shown in Figure 9d. In this case, a splitting into a multiple spot can also occur if the direction of propagation is not in perfect alignment with the edge.

Power transmission measurements for various guided-wave modes through a typical planar thin-slab waveguide (Figure 1) without the top microstrip electrode are plotted as a function of coupling angle with respect to waveguide normal in Figure 10. This experiment was performed with an input laser power at 3.5 W. Measurements of Figure 10 were made with a gaussian input laser beam ($\sigma = 0.75$ mm). The distance between the two prism couplers was 3 cm. Because of insufficient coupling length, the measured power transmission of the TE_0 mode (not shown in Figure 10) was only about 18%. The power transmission was highest for the TE_1 mode at 46%. These power transmission measurements are very reproducible for a number of similar waveguides evaluated at various input power levels up to 15 W. The variation in power transmission is less than 10% and is limited primarily by

LASER BEAM SHAPES

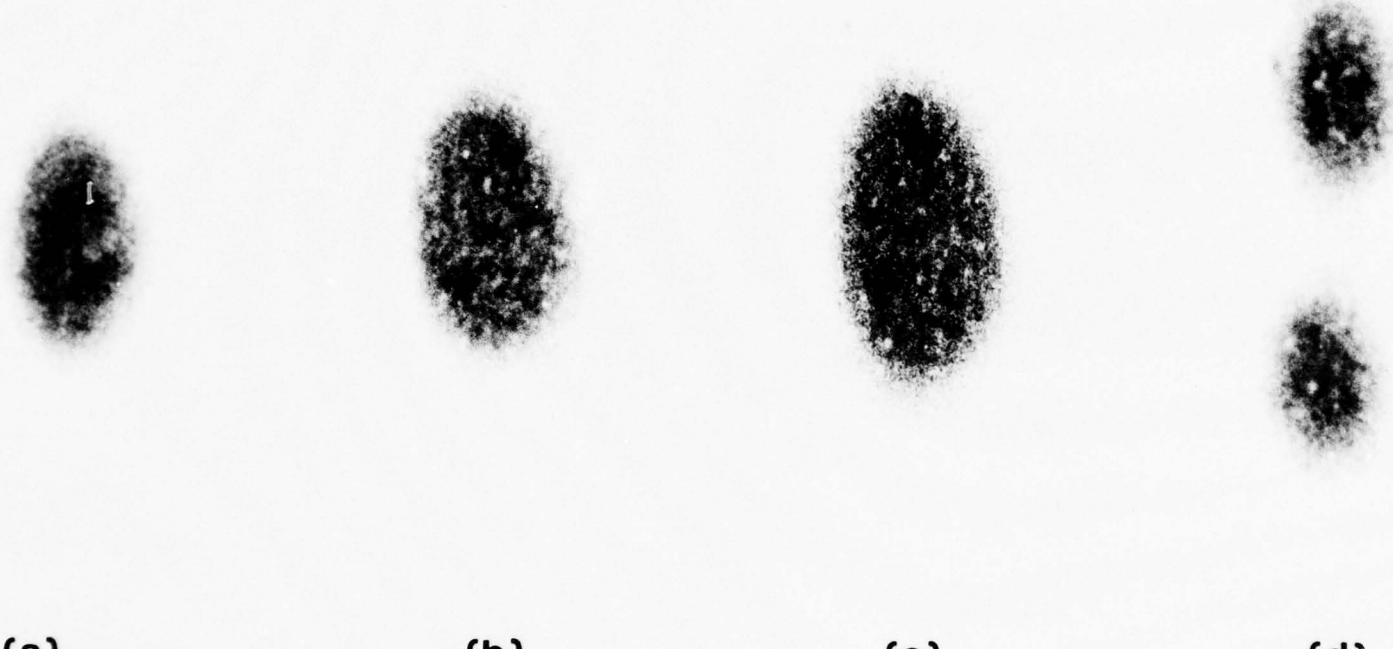

(a) (b) (c) (d)

FIG. 9

UNITED TECHNOLOGIES RESEARCH CENTER

UNITED TECHNOLOGIES

76-02-205-1

OPTICAL TRANSMISSION CHARACTERISTICS

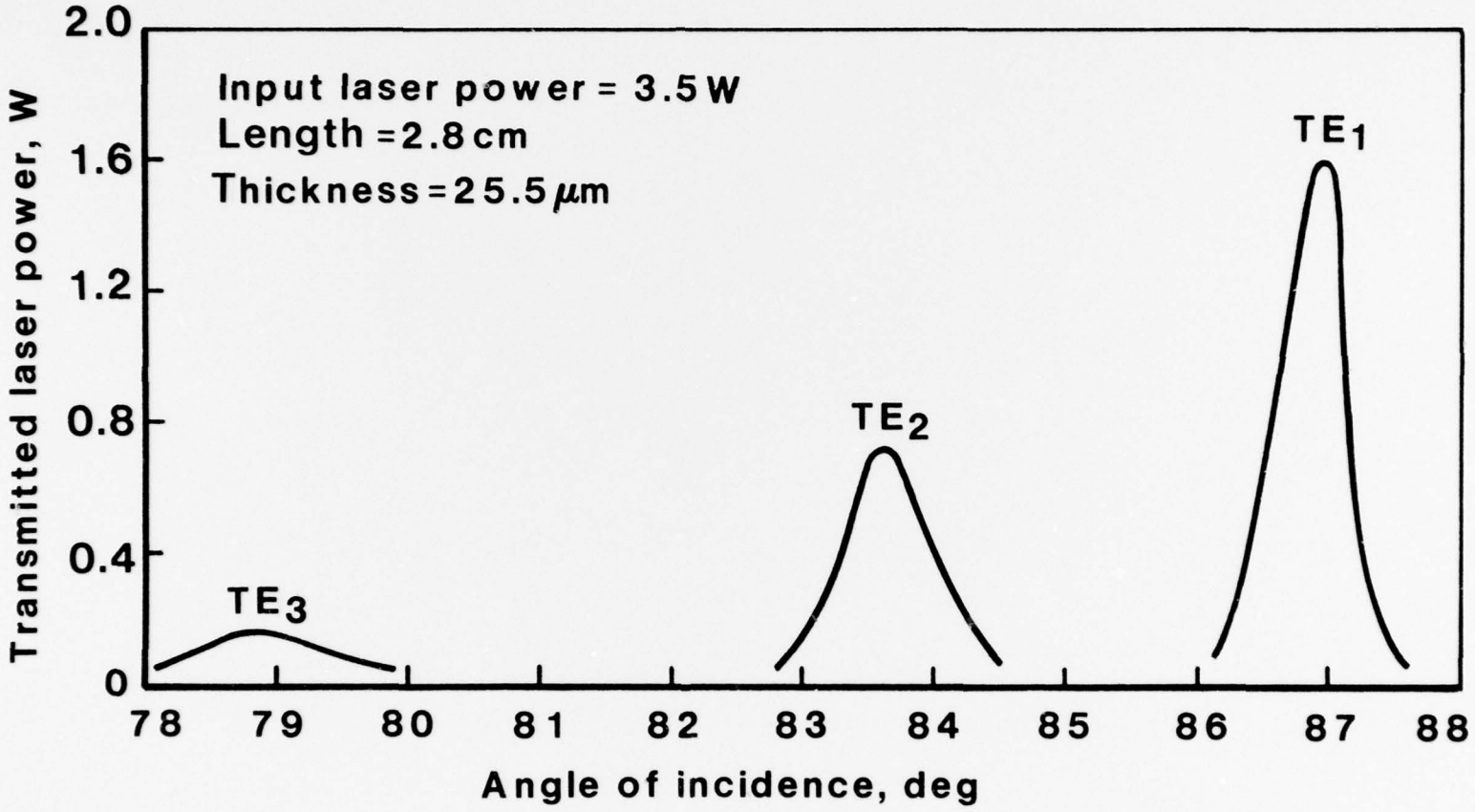

UNITED TECHNOLOGIES RESEARCH CENTER

R12-103-1

FIG. 10

the reproducibility of aperture-matched input laser beam shapes. Since the coupling efficiency and transmitted beam quality depends critically on the quality of the waveguides and the couplers, results obtained from these optical tests indicate that a high degree of structure uniformity has been achieved with these waveguides. The bases of the coupling prisms are optically flat and no attempt was made to create a varying coupling strength by means of a tapered gap spacing (Ref. 14). Therefore, the maximum theoretical transmission in our case is 81%, assuming a perfect (100%) output coupler. Furthermore, the gap-spacing for coupling of evanescent waves is always kept within 0.1 μm.

The results of Figure 10 show that the transmission for the higher-order modes (TE_1, etc.) for which nearly perfect aperture-matching can be achieved, is far below the optimum theoretical value of 81%. The sharp reduction in transmitted power for the higher order modes is caused primarily by electrode absorption at the metallic ground plane. To evaluate the power loss at the electrode, a top electrode (2.8 cm long) in a microstrip configuration was subsequently deposited on the surface of the waveguide. The measured transmission for the TE_1 mode is reduced from 46% to 33%. From these two power transmission measurements we obtain a value of 0.24 cm^{-1} for the absorption coefficient of the two electrodes for the TE_1 mode. Similarly we obtain a value of 0.05 cm^{-1} for the TE_0 mode. These results are in excellent agreement with the previously calculated values (Ref. 13). With these measurements we can estimate the input coupling coefficient from the transmission expression as given by

$$T = 0.92\ \eta\ e^{-3(\alpha_e + \alpha_m)}. \qquad (3)$$

Equation (3) has taken into account various losses, namely (1) the loss at two AR coated input and output prism faces, each of which reflects the laser power by about 4%, (2) the loss at the input prism with a coupling coefficient η (in all cases the output prism is assumed to be a perfect coupler), (3) the loss in a single electrode with an absorption coefficient α_e, and (4) the GaAs material absorption coefficient α_m at a known value of 0.01 cm^{-1}. From Eq. (3) we obtain an η value of 22% and 72% for the TE_0 mode and TE_1 mode, respectively. These values agree very well with the calculated values (Figure 4).

The measured power transmission results through a tapered waveguide are plotted in Figure 11 as a function of the coupling angle with respect to the waveguide normal. The total propagation length is 2.7 cm, of which a 2.1 cm long section of this waveguide is at a thickness of 25 μm. A length of approximately 3 mm is used for making the two tapered transitions and the remainder is used for the in and out coupling. The thickness of the coupling region is 13 μm. Because of the reduction of waveguide thickness in the coupling region, the model dispersion of the tapered waveguide is much greater than that of the planar waveguide

OPTICAL TRANSMISSION CHARACTERISTICS

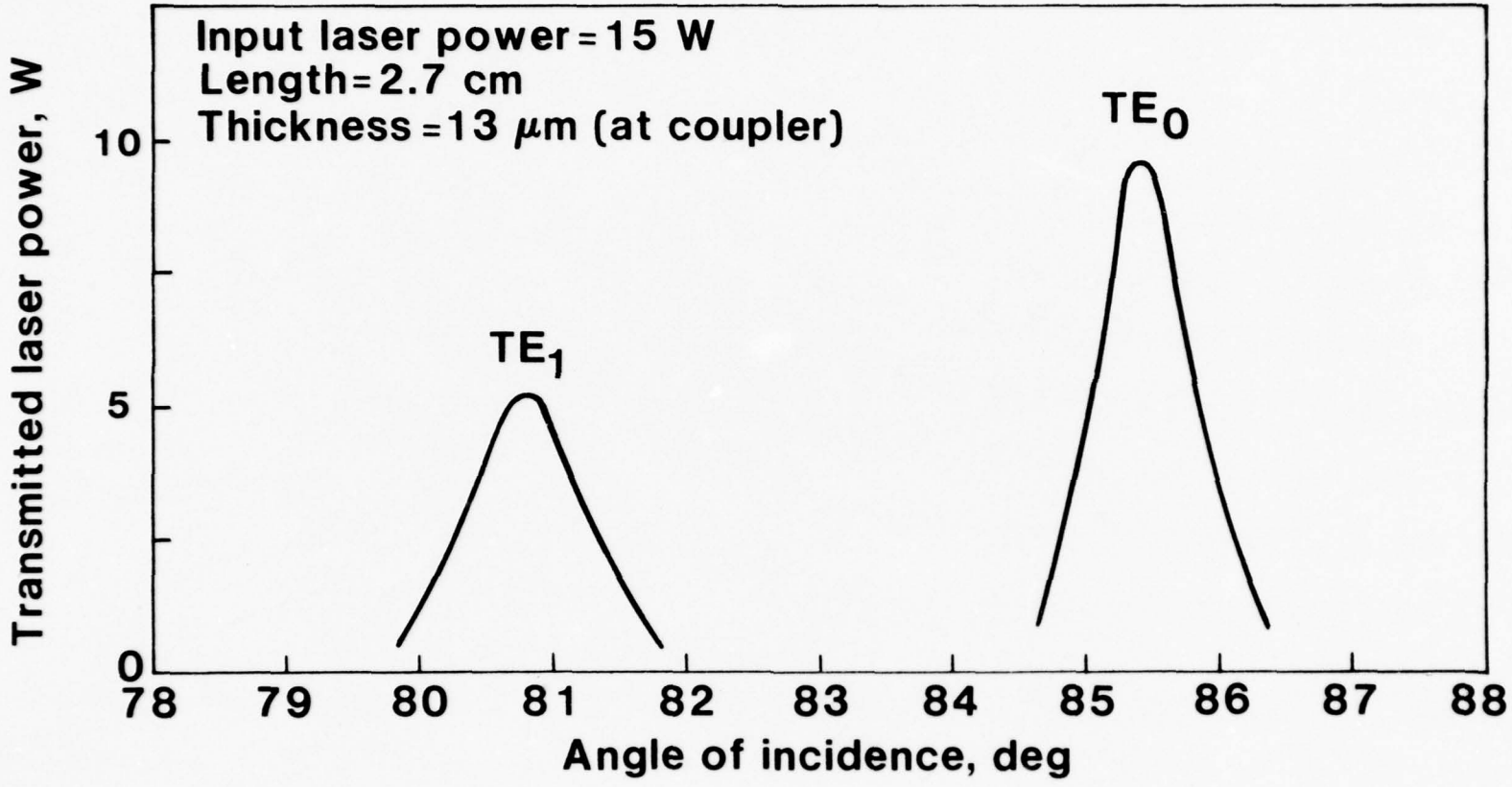

FIG. 11

UNITED TECHNOLOGIES RESEARCH CENTER

76-05-15-1

(Figure 10). The coupling angles for various modes of this tapered waveguide at the maximum transmission are found to be consistent with the calculated β/k values as shown in Figure 3, and provide the identification of these modes. The measured percent transmission for the TE_0 mode is 63.5 and that for the TE_1 mode is 29. By using Eq. (3) with the known loss values, the actual coupling efficiency is found to be 77.7% for the TE_0 mode and 48.6% for the TE_1 mode. These results are in excellent agreement with the calculated values plotted in Figure 4 for a waveguide thickness of 13 μm. The highest transmitted laser power is 9.5 W which corresponds to a power density of 80 kW/cm^2 at the input coupling region. This waveguide remains in a perfect condition after several hours of continuous operation at this power level.

3.5 Microwave Modulation of CO_2 Lasers

It was recognized early in this program that the best approach for obtaining the most efficient and broadband modulation of the high-power CO_2 laser is to excite and confine both the optical and microwave power in a common waveguide of the dimensions 25 μm thick, 1 mm wide and several centimeters long. With a proper design of the optical and microwave circuits, a large fraction of the laser power can be efficiently converted into the first sidebands which are up- and down-shifted at microwave frequencies by phase modulation (Ref. 9) of the 10 μm laser carrier.

The phase modulated carrier field can be expressed in a power expansion of Bessels functions, as given by (Ref. 20):

$$E = E_0 \left[(J_0(\Delta\phi) \sin(\omega_0 t + \phi_0) + J_1(\Delta\phi) \cos(\omega_0 t \pm \omega_\mu t + \phi_0) + \cdots \right] \quad (4)$$

where E_0, ω_0, ϕ_0 are the amplitude, angular frequency, and phase of the carrier, ω_μ is the microwave frequency and $\Delta\phi$ is the phase shift caused by the optical-microwave interaction in an electrooptic waveguide. For $\Delta\phi < 1$, the amplitude of the first upper and lower sidebands can be expressed by the approximation:

$$J_1(\Delta\phi) \simeq \Delta\phi/2. \quad (5)$$

The optical phase-shift, $\Delta\phi$ in Eq. 5, is directly proportional to the change of refractive index Δn of the waveguide as given by:

$$\Delta\phi = \left(\frac{2\pi}{\lambda}\right) dL\, \Delta n \quad (6)$$

where dL is a differential interaction length and λ is the laser wavelength. For long interaction lengths it is necessary to account for the differences in phase velocity between the optical beam and the microwaves and also, in particular, the microwave attenuation.

The change of refractive index for a TE mode propagating along either the (011) or $(0\bar{1}1)$ axis under an external field E_μ applied along the (100) axis is given by:

$$\Delta n = \left(1/2\right) n^3 \, r_{41} \, E_\mu \tag{7}$$

where $r_{41} = 1.2 \times 10^{-10}$ cm/V, and E_μ is determined by the circuit parameters and the microwave power.

Since the microwave circuit is unconventional in size compared to those commonly used for microwave components, it was necessary to determine experimentally the circuit parameters including the characteristic impedance, Z_0, the dielectric constant ε, and the attenuation coefficient, α. Parametric studies have been made for both the mini-gap ridge waveguides (Refs. 2, 3, 4) and the microstrip transmission lines (Refs. 6, 7). Results (Refs. 10, 11) indicate that both structures have nearly identical characteristics. In general, we found that the microstrip circuit is considerably better than the ridge structure in both reproducibility and reliability. These advantages are derived basically from a more precise control in fabrication of structural tolerances. The only disadvantage of using microstrip transmission line is its lower power handling capacity especially the matching network at its input port. The results indicated, however, that a small coaxial input line connected to the microstrip circuit can handle microwave power up to only 80 W. For continuous operation over a long time period at higher power level, a ridge waveguide would be the best choice.

The complete microwave microstrip circuit is shown in detail in Figure 12. The microwave power is center-fed through an input impedance transformer from a coaxial microstrip launcher and the ends are open circuited. The launcher, a standard design, was modified to have a longer center conductor extension with a semicircular shielding. The longer extension allowed the contact pressure to be distributed over a wider area on the GaAs thin-slab without causing material damage. The larger contact area for the microwaves also provided slight adjustments for improving the input impedance matching. With the center-feed excitation of the microstrip transmission line, only the wave that is in synchronous with the laser beam modulates the guided optical wave. At the center frequency the electrical distances are integral numbers of half wavelengths from the feedpoint to the open circuited ends. Although the configuration may seem narrow band, this is not necessarily the case. It turns out that if the feed line from a matched generator is well matched to the net characteristic impedance of the two lines in parallel,

IR Waveguide Modulator With A Standing-Wave Microstrip Electrode

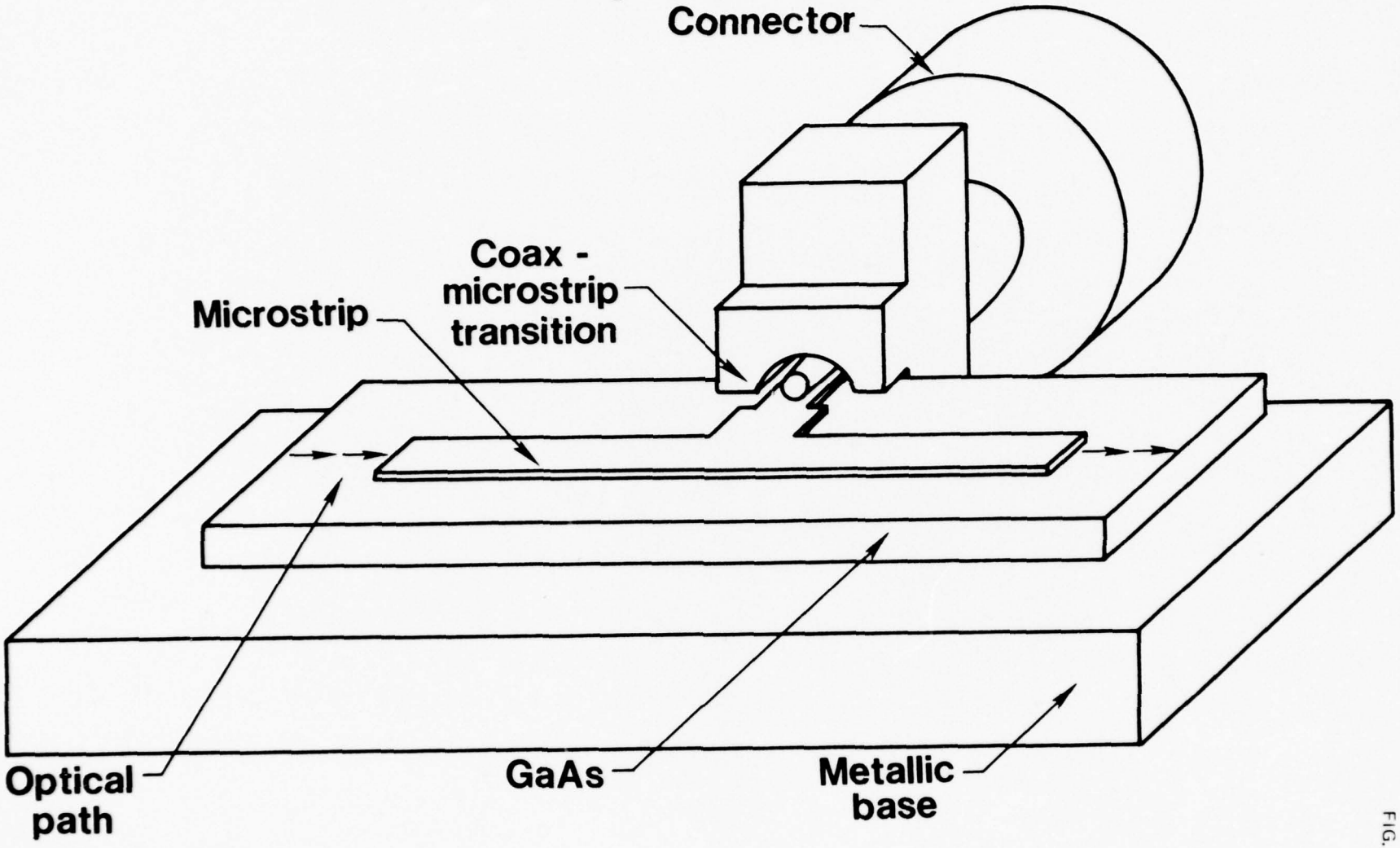

UNITED TECHNOLOGIES RESEARCH CENTER

FIG. 12

76-03-63-6

the amplitudes of the synchronous components of the standing wave are independent of frequency (Ref. 7). Therefore, a relatively broadband operation can be accomplished by placing a microwave circulator at the input port that not only protects the modulator driver but also produces a circuit almost equivalent to that of a two port modulator. The most efficient modulation condition, of course, occurs when the net input resistance is transformed so that an impedance match exists at the input port of the modulator. Under these matched conditions, the power in the first sidebands is given, from Eq. 5, as:

$$P_{SB} = \left(\frac{\Delta\phi}{2}\right)^2 P_O \tag{8}$$

in which the phase shift $\Delta\phi$ is given by the expression (Ref. 3) (with the assumption that both the optical and the microwave fields are in synchronism)

$$\Delta\phi = \frac{\pi}{2\lambda} r_{41} n^3 \left(\frac{2P_\mu \xi L}{tw\alpha}\right)^{1/2} \tag{9}$$

where P_O and P_μ are the laser and microwave power, respectively. w is the width of the microstrip line, $\xi = \sqrt{\mu/\epsilon} = 377/3.5$ ohm, α is the microwave attenuation (in nepers per unit length), and other symbols as previously defined.

Figure 13 is a photograph of a standing-wave waveguide modulator. As shown in this picture, the input impedance transformer is made of a one-quarter-wave-long microstrip line with a selected impedance value. The transformer ratio commonly used in our work is about 4 to 1 for the matching of a 50 ohm generator impedance down to about 12 ohm, which is the input impedance of the resonant microstrip line. The characteristic impedance of the modulator is 2.7 ohm.

The measurements of sideband power as a function of microwave frequency are shown in Figure 14. The measured modulation bandwidth and conversion efficiency are nominally 700 MHz and 0.7%, respectively, for a 2.78 cm long ($\sim 5\ \lambda_\mu$) modulator at an input microwave power of 20 W. These measurements are consistent with the calculated results by assuming a total loss of 2 dB in the microstrip transmission line.

Because of the length of the microstrip line there should exist a series of resonances. By using another 2.8 cm long microstrip modulator with a center-feed input impedance transformer designed for 15 GHz, we have obtained the sideband power at various resonant frequencies, 9.9 GHz, 12.3 GHz, 15.0 GHz and 17.8 GHz, which correspond to 3 λ_μ, 4 λ_μ, 5 λ_μ and 6 λ_μ, respectively. The measurements of the relative sideband power at each resonance are shown in Figure 15. It is interesting to note that the measured sideband power is higher at 12.3 GHz than

Standing-wave Microstrip Waveguide Modulator Element

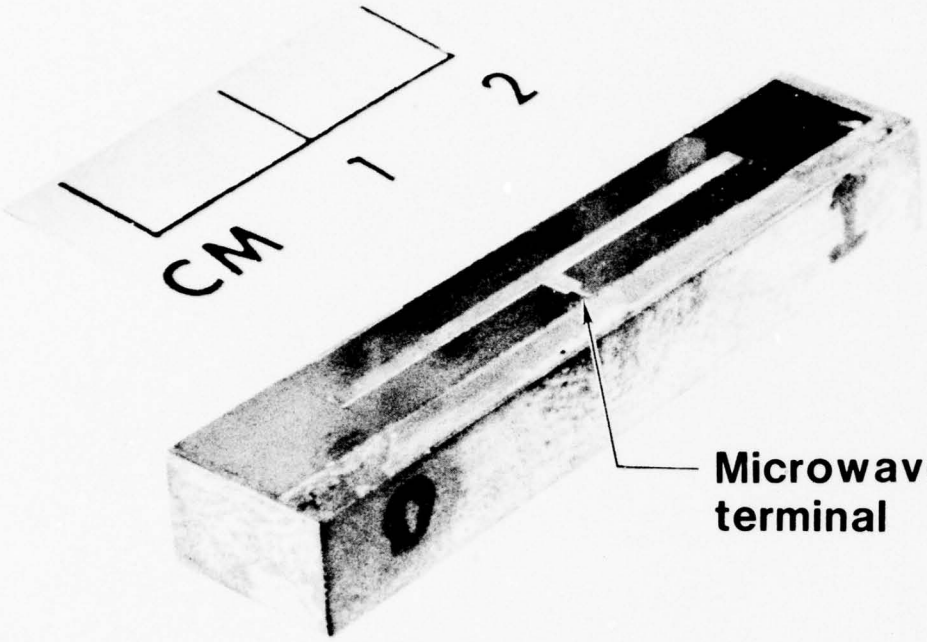

UNITED TECHNOLOGIES RESEARCH CENTER

FIG. 13

76-09-36-2

MODULATOR FREQUENCY RESPONSE

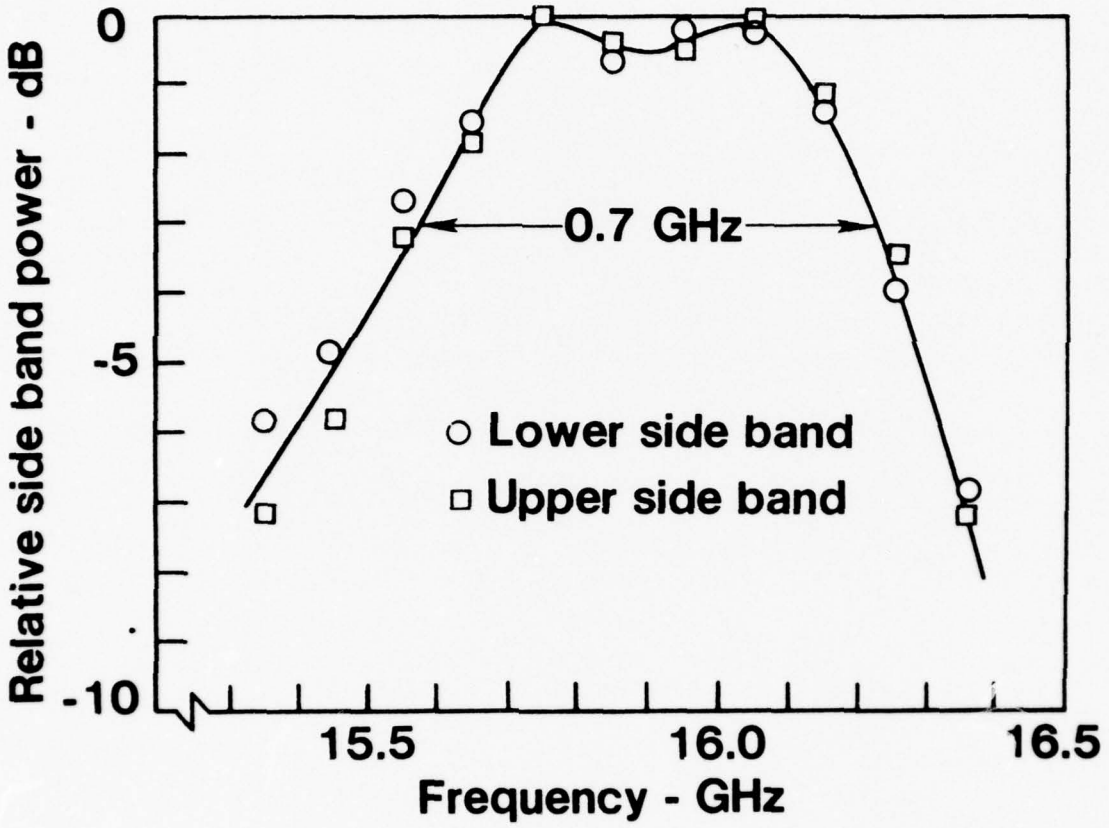

UNITED TECHNOLOGIES RESEARCH CENTER

FIG. 14

76-03-63-5

Frequency Response of a Center-Feed Waveguide Modulator

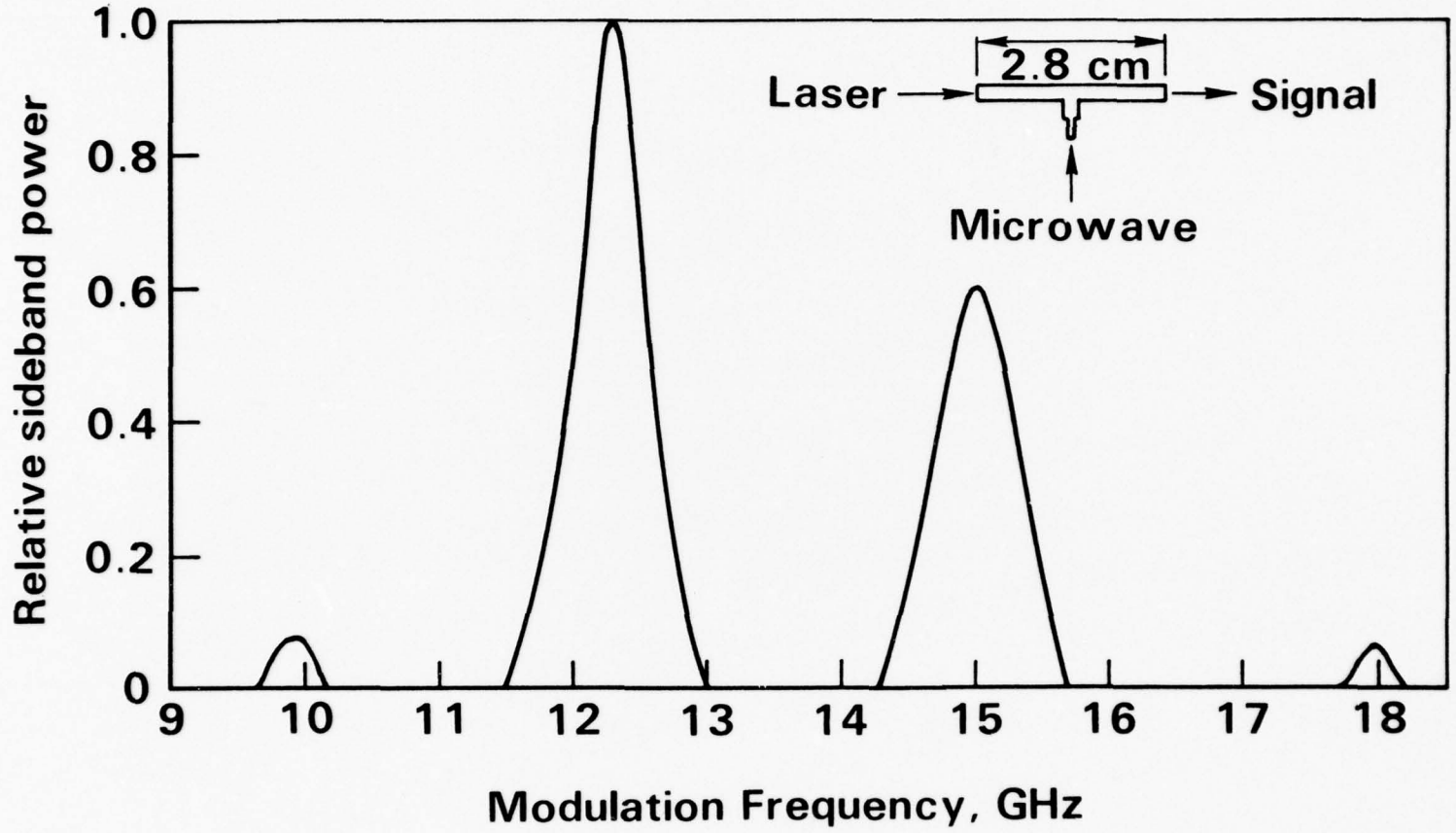

FIG. 15

UNITED TECHNOLOGIES RESEARCH CENTER

76-08-225-1

that at 15 GHz, which is the design frequency. This suggests that the circuit loss at 12.5 GHz is about 0.4 dB/cm as compared with 0.7 dB/cm at 15 GHz. The roll-off in sideband power at the two extreme points is expected because the length ($\lambda/4$) of the input transformer is selected to favor the 15 GHz resonance.

Although most of our modulation experiments were carried out at a laser carrier power of about 4 W and an applied microwave power of 20 W, the structure has been operated at 15 W of laser power and 80 W of microwave power. The sideband signals are displayed by using an electronically scanning Fabry-Perot filter. A typical signal from the scanning filter is shown in Figure 16. The spacing between the two peaks corresponds to 32 GHz and the full scan is 50 GHz.

With a high power microwave TWT amplifier, we have obtained optical sideband power conversion efficiency as high as 2.1% by increasing the microwave power to 60 W. Figure 17 is a plot of the measured conversion efficiency as a function of the microwave power. Results clearly indicate that a linear dependence of the sideband conversion efficiency on the microwave power up to 60 W is obtainable with this waveguide modulator. Above 80 W, an electrical breakdown occurred at the narrowest section of the microstrip step transformer (≃ 13 mil wide). As mentioned before, a ridge waveguide must be used as the input line for operation at high power levels. Based upon the present state-of-the-art, it is now possible to obtain as high as 0.3 W of single sideband power at 16 GHz with a 20 W CO_2 laser and 60 W microwave source as the inputs to a GaAs thin-slab waveguide modulator.

Because of the moderate loss in the 25 μm thick and one millimeter wide microstrip circuit, the use of narrow-band standing-wave modulator structure does not appear to offer much enhancement in conversion efficiency than that expected from a broadband traveling-wave design. A theoretical design of a broadband waveguide modulator is presented in the following paragraphs. However, the important problems which remain to be determined are in the implementation and in the fabrication of the desired circuit. At microwave frequencies broadband impedance transformers are realized by connecting in tandem a series of transmission lines which are one-quarter wavelength long at the center frequency and which have a prescribed set of values for characteristic impedance. A similar technique is used for AR coating in optical devices; however, there is more flexibility with microwave transmission lines because the transverse dimensions of the lines are adjustable parameters. Thus, a continuum of values for characteristic impedance within practical limits can be achieved.

For the broadband modulator design, the modulator characteristic impedance must be known. For a one mil thick and 1 mm wide metallic strip, the characteristic impedance has been determined to be 2.7 ohm and its attenuation has been determined to be 0.4 dB per wavelength at 16 GHz. An effective index of refraction was found to be 3.5. Because the thickness of this microstrip transmission line

Spectral Characterestics Of A Modulated CO_2 Laser Output

Input power: 60 W Efficiency: 2%

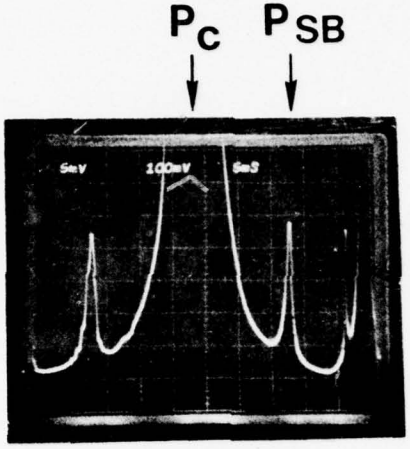

UNITED TECHNOLOGIES RESEARCH CENTER

FIG. 16

76-04-318-2

POWER DEPENDENCE OF SIDEBAND CONVERSION EFFICIENCY

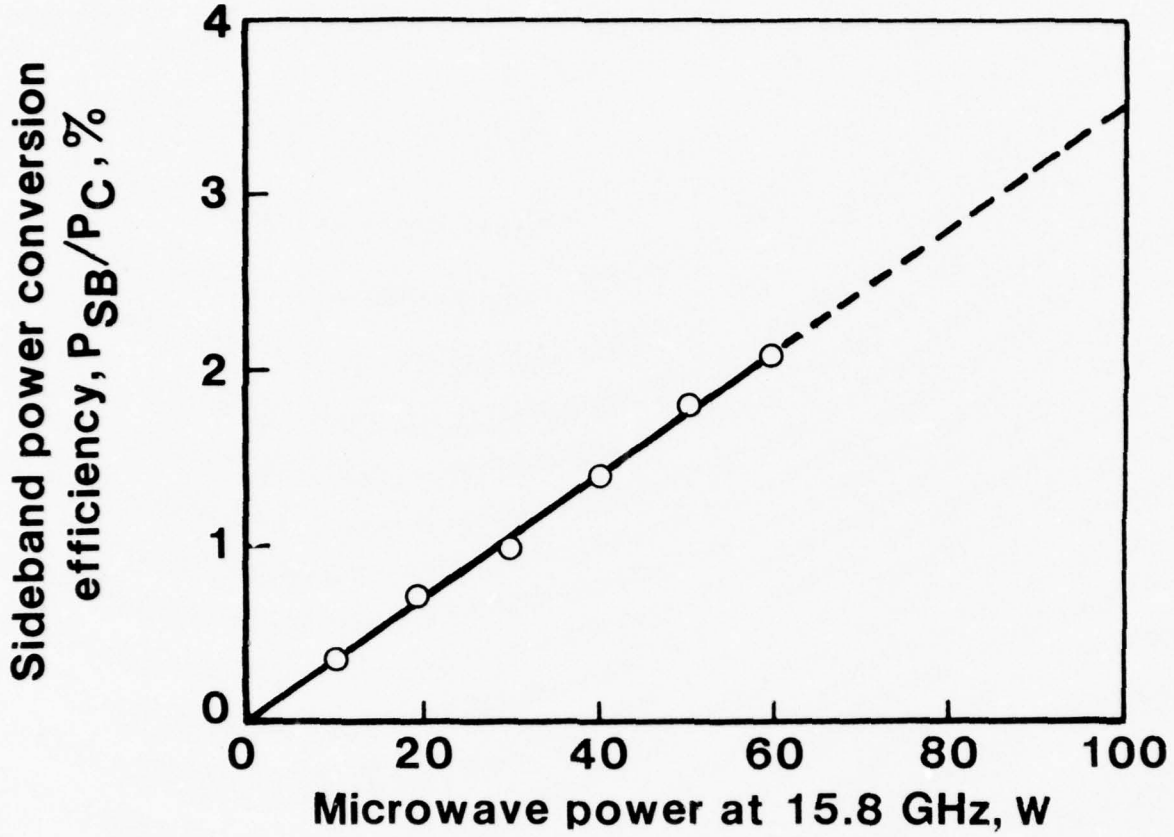

UNITED TECHNOLOGIES RESEARCH CENTER

76-03-232-1

FIG. 17

is only one mil, which is very small as compared with the microwave wavelength, experimental procedures for determining the above characteristics become very difficult. The measurement depends upon fabrication techniques and the intermediate circuit components which are required to make the transition from the extremely small modulator dimensions to standard microwave components of relatively large sizes.

An analysis has been made of the frequency characteristics of the broadband microwave modulator using a theoretical model with the assumption that small junction parasitic reactances can be accounted for by small corrections in the physical lengths of the acutal elements. The microwave circuit model of the modulator is sketched in Figure 18. This model, a traveling wave configuration, consists of the main transmission line of length L and two identical impedance transformers at each end. Each transformer contains three one-quarter wavelength steps with impedance values selected to give a maximally flat response. These transitions involve several dimensional changes in the microstrip configuration. An additional component, R_L = 10,000 ohm, was added at the center of the line as a mathematical device to permit the calculation of the voltage across the line. The relatively large value of R_L makes its effect negligible electrically. Under the assumption that a synchronous condition exists between the microwave and the IR radiation, the degree of modulation depends only upon the distribution of synchronous wave amplitude along the modulator. Thus, the voltage at the midpoint of the line can be used to approximate the average amplitude of the synchronous wave over the frequency range of interest. Since the power generated in the optical sidebands is proportional to power carried by the synchronous component of the microwaves, the modulator performance is proportional to the ratio of the synchronous microwave power to that available from the microwave power source at the input terminals of the modulator.

The detailed calculations of the frequency response of the modulator are fairly tedious because each section of transmission must be handled separately through the well known microwave transmission line equations which involve sums of hyperbolic functions with complex arguments and coefficients. The calculations are further complicated by the attenuation coefficients which varies noticeably with frequency. A general computer program designed for microwave circuits, which is an advanced form of one designed by P. E. Green (Ref. 21), has been applied to this modulator problem. In the calculations, the power delivered to R_L was first calculated at each frequency and then converted to the equivalent power value for a synchronous wave that would produce the same voltage, V_n at the midpoint. The results are plotted in Figure 19 for an active modulator length of 2.78 cm (5 wavelengths at 16 GHz), for a frequency range extending from 6 to 26 GHz. The useful range is the 8 GHz band indicated by the solid section of the curve drawn in Figure 19. The dashed sections of the curve are not useful regions of operation because of rapid variations. The useful range is shown in Figure 20 on an expanded frequency scale. The calculated results as given by a

MODEL OF WIDEBAND MICROWAVE MODULATOR

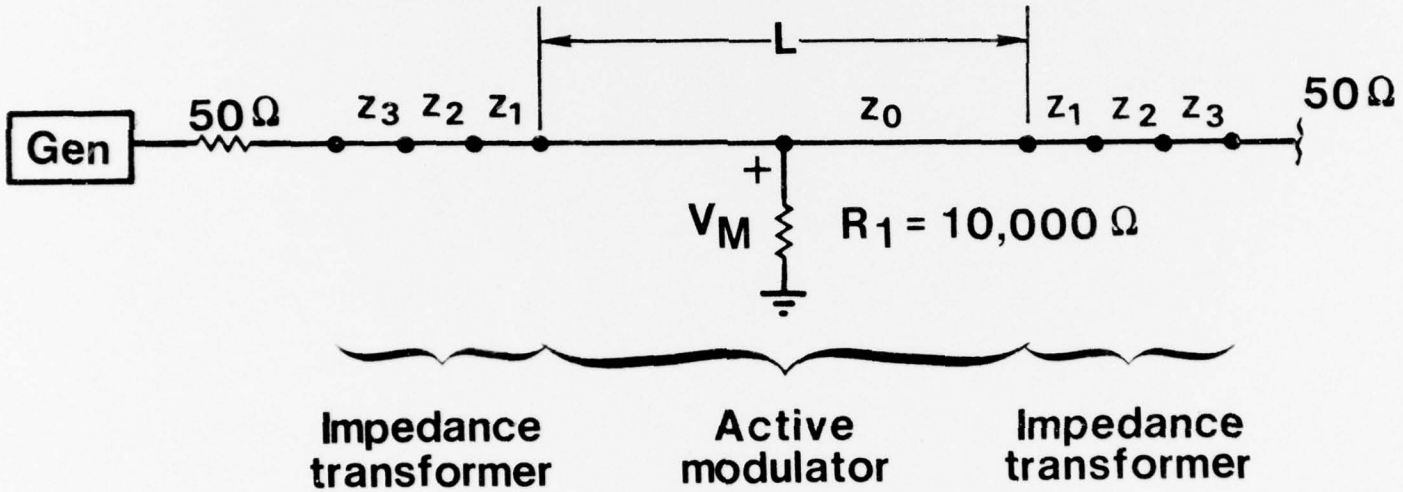

FIG. 18

76-05-125-4

UNITED TECHNOLOGIES RESEARCH CENTER

THEORETICAL WIDEBAND RESPONSE OF MICROWAVE MODULATOR

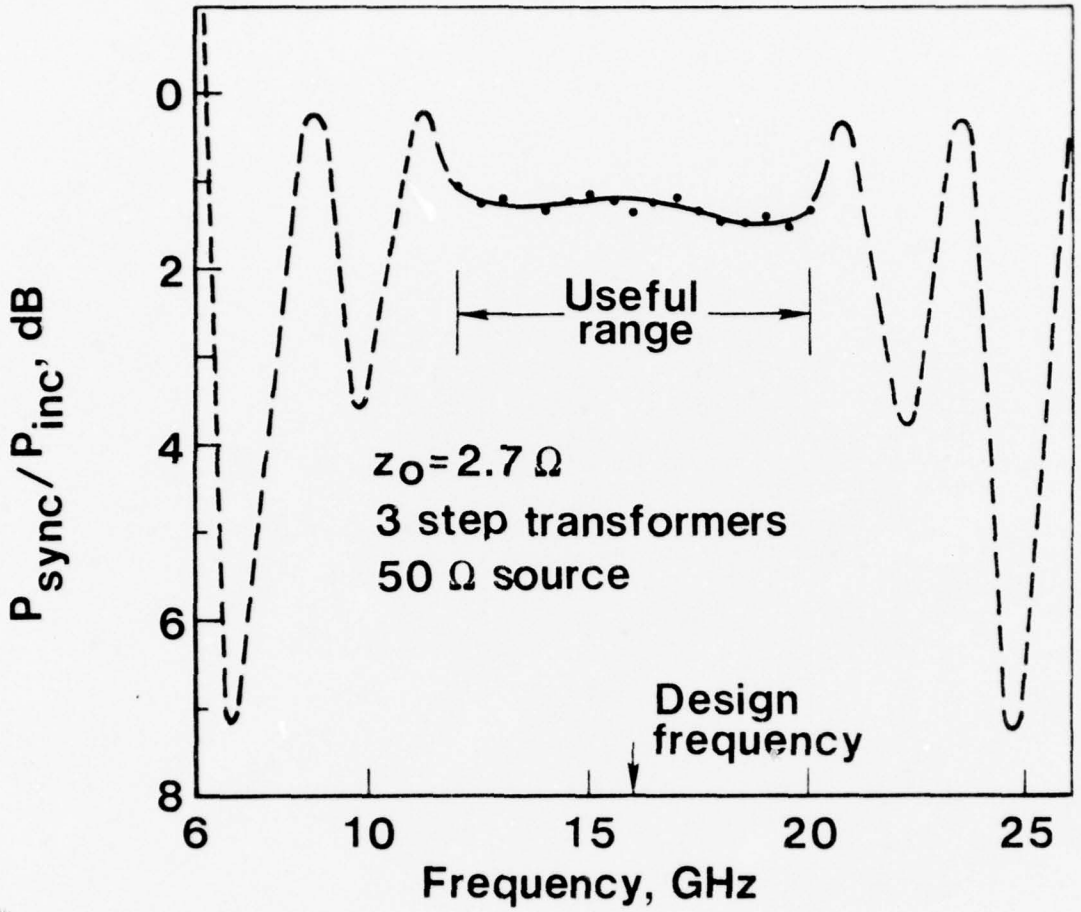

FIG. 19

UNITED TECHNOLOGIES RESEARCH CENTER

76-05-125-1

THEORETICAL PASSBAND RESPONSE OF MICROWAVE MODULATOR

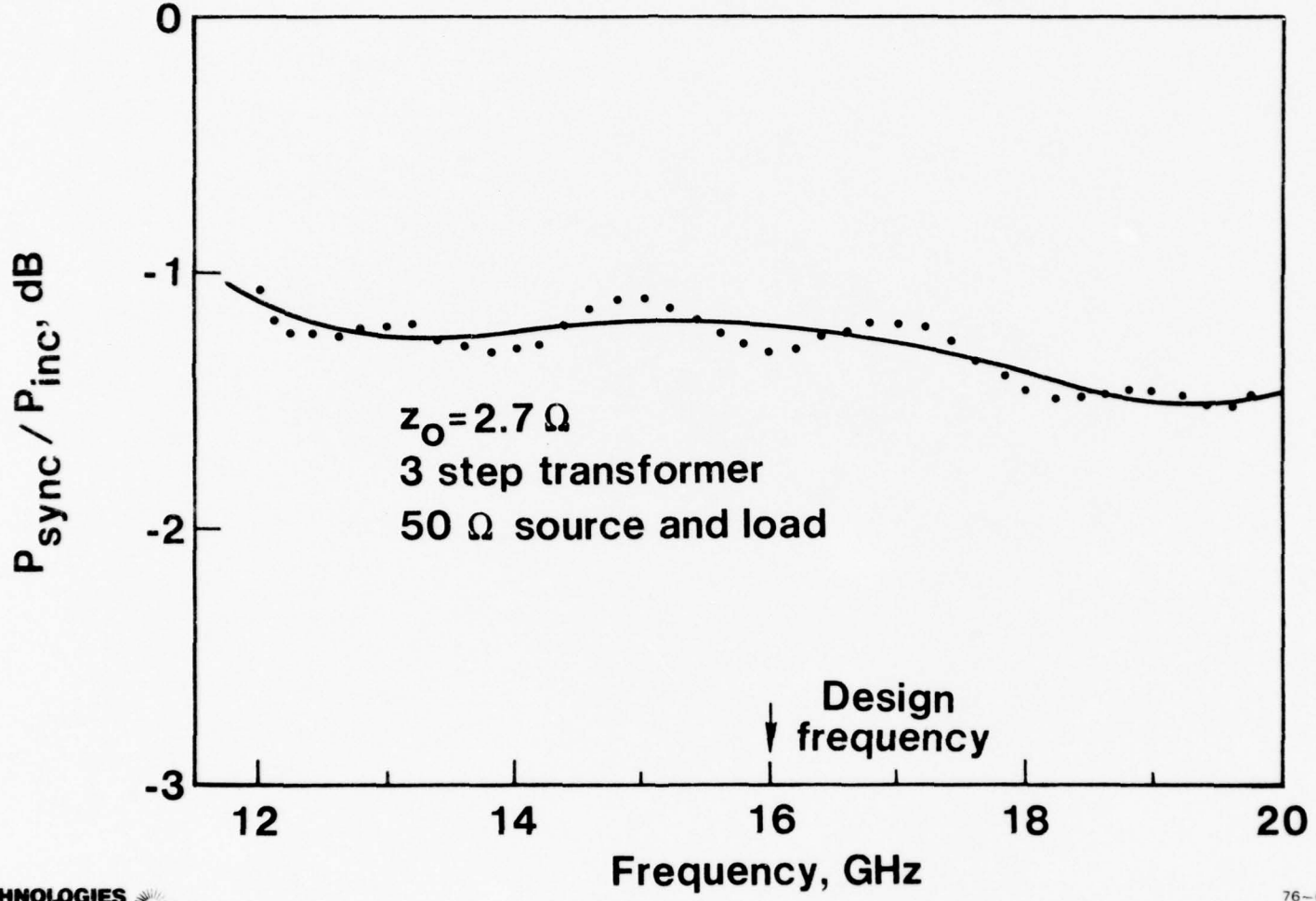

FIG. 20

76-05-125-2

UNITED TECHNOLOGIES RESEARCH CENTER

series of points define a curve with many ripples which in themselves are not completely representative of the amplitude response of the synchronous wave. The method of calculation described above does not distinguish between the contributions from the synchronous wave and from a small reflected wave. The reflected wave must be present since the impedance transformers at the ends are never perfect. Examination of the calculated data points in Figure 20 shows that the periodicity is approximately 2 GHz value, which is of the right order of magnitude corresponding to reflections from two discontinuities spaced 5 wavelengths at 16 GHz, the design frequency. A representative variation of the amplitude of the synchronous wave with frequency is thus obtained by averaging out these ripples. The total variation in the ratio of synchronous power to incident power in the useful range is less than 0.5 dB with lower values falling at the high end of the frequency range because of higher attenuation there. The mean level of approximately -1.25 dB is consistent with the microwave attenuation being a total of 2 dB for 5 wavelengths at 16 GHz.

Experimentally we have obtained a broadband turning of a CO_2 laser continuously over a spectral range from 9 GHz to 18 GHz, by using a traveling-wave waveguide modulator as shown in Figure 21. The optical structure of this modulator is similar to that of the standing-wave modulators, except that the microwave power is fed from one end of the microstrip electrode, which has a three-step transformer at its input terminal. The transformer network is made by connecting a 12 mil thick GaAs slab to the 1 mil GaAs waveguide. At the transition, the microstrip electrode configuration of this first experimental model has not been made precisely as specified by the design, nevertheless, it allows a reasonable amount of microwave input power to be fed into the microstrip transmission line over the entire Ku-band. With this modulator, we have measured the optical sideband power as a function of the modulation frequency. Figure 22 shows the normalized frequency response of this first traveling-wave waveguide modulator. The results indicate that continuous tuning of a CO_2 laser over very broad frequency range is obtainable with a traveling-wave waveguide modulator and the maximum sideband power is about one-third that of the standing-wave case. The series of resonant peaks seen in Figure 22 is caused primarily by the imperfection of the three-step transformer, and can be eliminated by further improvement of fabrication techniques.

Traveling–Wave Microstrip Waveguide Modulator

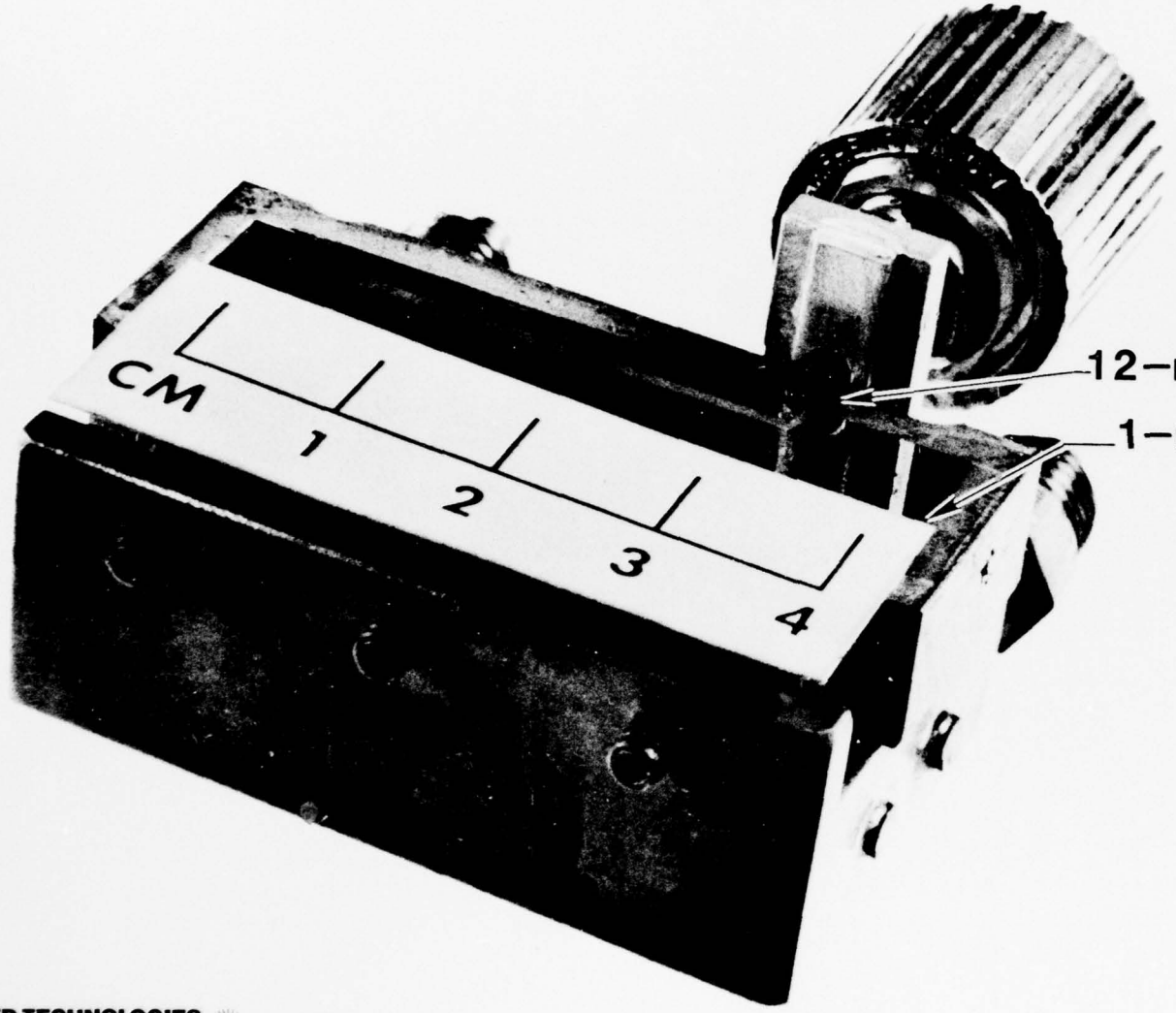

UNITED TECHNOLOGIES RESEARCH CENTER

UNITED TECHNOLOGIES

76–09–240–1

FIG 21

Frequency Response of a Traveling-Wave Waveguide Modulator

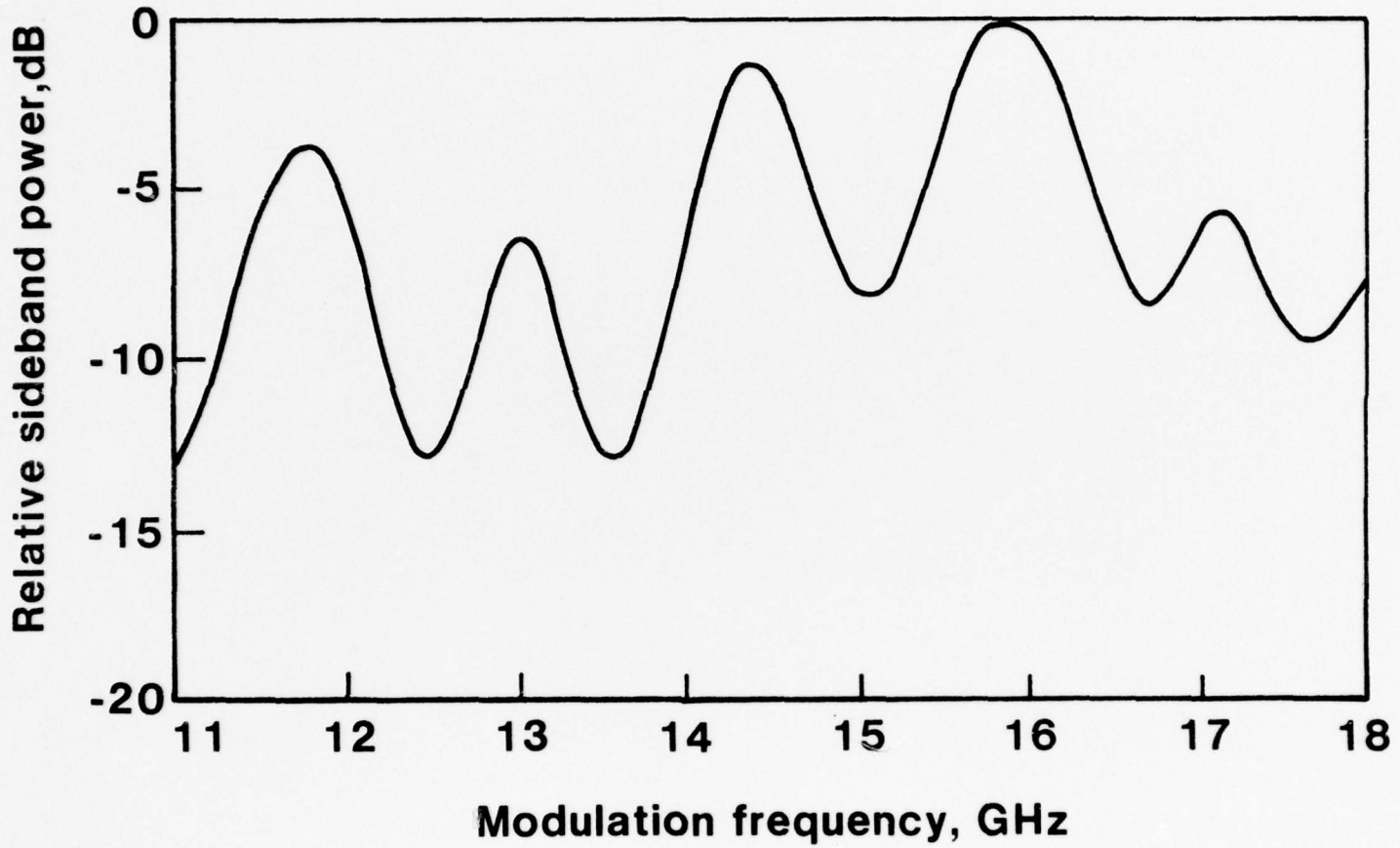

FIG. 22

4.0 CONCLUSIONS

Techniques have been developed to produce reliably high power infrared waveguides suitable for broadband modulation of CO_2 laser radiation. Optical power transmission through a 3 cm long metal-cladded and tapered thin-slab waveguide at a thickness of 25 μm was found to be greater than 60% which is approaching that expected from a bulk GaAs crystal of identical length. The difference in optical power transmission between the waveguide and bulk modulator devices is insignificant in comparison with the enhancement (~ 20 dB gain) in the electric field strength which can be generated by using the waveguide device instead of a bulk device with the same amount of modulation power. With a standing-wave waveguide structure, we have obtained 2.1% power conversion efficiency from the carrier to a single sideband by applying 60 W microwave power to a 2.8 cm long microstrip electrode. The modulation bandwidth of a standing wave structure is nominally 1 GHz. By using a traveling-wave structure with a three-step transformer network, a factor of ten increase in modulation bandwidth has been achieved by sacrificing the conversion efficiency by about a factor of three. It may be possible to increase the electrooptic effect by using CdTe as the waveguide material. In this work, GaAs was used primarily because high quality, large-size ingots are readily available. Nevertheless, techniques developed for GaAs should also be applicable to CdTe.

The authors wish to thank W. Glueck and R. Rukus for technical assistance. They are grateful to Dr. M. White for helpful discussions.

5.0 REFERENCES

1. Cheo, P. K.: Investigation of Thin-Film Modulator for 10 Micron-Lasers. UARL Interim Technical Report, M-921513-2, March 30, 1973.

2. Cheo, P. K., M. Gilden, J. F. Black and J. L. Swindal: Ultra-Wideband Thin-Film Modulator for CO_2 Lasers. UARL Semi-Annual Technical Report M-921513-4, September 30, 1973.

3. Cheo, P. K., M. Gilden, D. W. Fradin, and R. Wagner: Microwave Modulation of CO_2 Laser in GaAs Thin-Film Optical Waveguides. UARL Third Semi-Annual Technical Report, N921513-6, March 29, 1974.

4. Cheo, P. K., M. Gilden, D. W. Fradin, and R. Wagner: Microwave Waveguide Modulators for CO_2 Lasers. UARL Fourth Semi-Annual Technical Report N921513-8, September 25, 1974.

5. Cheo, P. K., D. W. Fradin, and R. Wagner: Microwave Waveguide Modulators for CO_2 Lasers. UARL Fifth Semi-Annual Technical Report R921513-10, March 31, 1975.

6. Cheo, P. K., M. Gilden, and R. Wagner: Infrared Waveguide Modulators at Microwave Frequencies. UTRC Sixth Semi-Annual Technical Report R75-922241-1, September 30, 1975.

7. Cheo, P. K., D. W. Fradin, M. Gilden, and R. Wagner: High Power Infrared Waveguide Modulators. UTRC Seventh Semi-Annual Technical Report R76-922241-3, March 30, 1976.

8. Cheo, P. K.: Pulse Amplitude Modulation of a CO_2 Laser in an Electrooptic Thin-Film Waveguide. Appl. Phys. Lett., 22, 241 (1973).

9. Cheo, P. K.: Electrooptic Properties of Reverse-Biased GaAs Expitaxial Thin Films at 10.6 μm. Appl. Phys. Lett., 23, 439 (1973).

10. Cheo, P. K. and M. Gilden: Microwave Modulation of CO_2 Lasers in GaAs Optical Waveguides. Appl. Phys. Lett., 25, 272 (1974).

11. Cheo, P. K. and M. Gilden: High Power Integrated Optic IR Modulator at Microwave Frequencies. Appl. Phys. Lett., 28, 626 (1976).

12. Cheo, P. K. and R. Wagner: Infrared Electrooptic Waveguides. J. Quant. Electronics, (to be published).

REFERENCES (Cont'd)

13. Cheo, P. K., J. M. Berak, W. Oskinsky, and J. L. Swindal: Optical Waveguide Structures for CO_2 Lasers. Appl. Optics, 12, 500 (1973).

14. Tien, P. K.: Light Waves in Thin Films and Integrated Optics. Appl. Optics, 10, 2395 (1971).

15. Chang, M. S., W. S. C. Chang, B. L. Sopori, H. R. Vann, M. W. Muller, M. G. Craford, D. Finn, W. O. Groves, and A. H. Herzog: GaAs Optical Waveguide Structures at 10.6 μm Wavelength. Appl. Optics, 14, 1572 (1975).

16. Spears, D. L., A. J. Strauss, S. R. Chinn, I. Melngailis, and P. Vohl: Integrated Optics Tech. Digest, January 12-14, 1976, Paper TuD3.

17. Lotspeich, J. F.: Single Crystal Electrooptic Thin-Film Waveguide Modulators for Infrared Laser Systems. Appl. Optics, 13, 2529 (1974).

18. Tien, P. K. and R. Ulrich: Theory of Prism-Film Coupler and Thin-Film Light Guides. J. Opt. Soc. Am., 60, 1325 (1970).

19. Kaminow, I. P. and E. H. Turner: Electrooptic Light Modulators. Proc. IEEE, 54, 1374 (1966).

20. Goldman, S.: Frequency Analysis, Modulation and Noise. McGraw Hill Book Co., Chap. 5, (1948).

21. Yound, L.: Tables for Cascaded Homogeneous Quarter-Wave Transformers. E.R.E. Trans. MIT-7, 233 (1959).

DISTRIBUTION LIST - R76-922241-4

Office of Naval Research Department of the Navy Attn: Physics Program Arlington, Virginia 22217	3 Copies
Naval Research Laboratory Department of the Navy Attn: Technical Library Washington, D. C. 20375	1 Copy
Office of the Director of Defense Research and Engineering Information Office Library Branch The Pentagon Washington, D. C. 20301	1 Copy
U. S. Army Research Office Box CM Duke Station Durham, North Carolina	1 Copy
Defense Documentation Center Cameron Station Alexandria, Virginia 22314	12 Copies
Defender Information Analysis Center Battelle Memorial Institute 505 King Avenue Columbus, Ohio 43201	1 Copy
Director Office of Naval Research Branch Office 536 South Clark Street Chicago, Illinois 60615	1 Copy
San Francisco Area Office Office of Naval Research 760 Market Street, Room 447 San Francisco, California 94102	1 Copy
Air Force Office of Scientific Research Department of the Air Force Washington, D. C. 22209	1 Copy

Office of Naval Research Branch Office — 1 Copy
Attn: Dr. Robert Behringer
1030 East Green Street
Pasadena, California 91106

Code 102 1P (ONRL) — 6 Copies
Office of Naval Research
800 N. Quincy Street
Arlington, Virginia 22217

Defense Advanced Research Projects Agency — 2 Copies
1400 Wilson Blvd.
Arlington, Virginia 22209
Attn: Director, Laser Division
Dr. P. Clark

ODDR&E — 1 Copy
Pentagon
Washington, D. C. 20301
Attn: Ass't Dir. (Space and Advanced Systems) — 1 Copy

Office of the Ass't Secretary of Defense — 1 Copy
System Analysis (Strategic Programs)
Washington, D. C. 20301
Attn: Mr. Gerald R. McNichols

U. S. Arms Control and Disarmament Agency — 1 Copy
Dept. of State Bldg., RM 4931
Washington, D. C. 20451
Attn: Dr. Charles Henkin

Energy Research Development Agency — 1 Copy
Division of Military Applications
Washington, D. C. 20545

National Aeronautics and Space Administration — 1 Copy
Lewis Research Center
Cleveland, Ohio 44135
Attn: Dr. John W. Dunning, Jr.
(Aerospace Res. Engineer)

National Aeronautics & Space Administration — 1 Copy
Code RR, FOB 10B
600 Independence Ave. SW
Washington, D. C. 20546

National Aeronautics and Space Administration
Ames Research Center
Moffet Field, California 94035
Attn: Mr. Robert L. McKenzie — 1 Copy
Dr. Kenneth W. Billman — 1 Copy

Department of the Army
Office of the Chief of RD&A
Washington, D. C. 20310
Attn: DARD-DD — 1 Copy
DAMA-WSM-T — 1 Copy

Department of the Army — 2 Copies
Office of the Deputy Chief of Staff
For Operations & Plans
Washington, D. C. 20310
Attn: DAMO-RQD

Ballistic Missile Defense Program Office (BMDPO) — 3 Copies
The Commonwealth Bldg.
1300 Wilson Blvd.
Arlington, Virginia 22209
Attn: Mr. Albert J. Bast, Jr.

U. S. Army Missile Command — 2 Copies
Research and Development Division
Redstone Arsenal, Alabama 35809
Attn: Army High Laser Energy Programs

Commander — 1 Copy
Rock Island Arsenal
Rock Island, Illinois 61201
Attn: SARRI-LR, Mr. J. W. McGarvey

Commanding Officer — 1 Copy
U. S. Army Mobility Equipment R&D Center
Ft. Belvior, Virginia 22060
Attn: SMEFB-MV

Commander — 1 Copy
U. S. Army Armament Command
Attn: AMSAR-RDT
Rock Island, Illinois 61201

Director
Ballistic Missle Defense Advanced Technology Center
P. O. Box 1500
Juntsville, Alabama 35807
Attn: ATC-O — 1 Copy
ACT-T — 1 Copy

Commander
U. S. Army Material Command
Alexandria, Virginia 22304
Attn: Mr. Paul Chernoff (AMCRD-T) — 1 Copy
Dr. B. Zarwyn (AMCRD-T) — 1 Copy

Commanding General — 1 Copy
U. S. Army Munitions Command
Dover, New Hampshire 07801
Attn: Mr. Gilbert F. Chesnov (AMSMU-R)

Director
U. S. Army Ballistic Res. Lab
Aberdeen Proving Ground, MD 21005
Attn: Dr. Robert Eichelberger — 1 Copy
Mr. Frank Allen — 1 Copy
Dr. E. C. Alcarez — 1 Copy

Commandant
U. S. Army
Air Defense School
Ft. Bliss, Texas 79916
Attn: Air Defense Agency — 1 Copy
ATSA-CTD-MS — 1 Copy

Commanding General
U. S. Army Combat Dev. Command
Ft. Belvoir, Virginia 22060
Attn: Director of Material, Missile Div. — 1 Copy

Commander — 1 Copy
U. S. Army Training and Doctrine Command
Attn: ATCD-CF
Ft. Monroe, Virginia 23651

Commander — 1 Copy
U. S. Army Electronics Command
Ft. Monmouth, New Jersey 07703
Attn: AMSEL-CT-L, Dr. R. G. Buser

Commander — 1 Copy
U. S. Army Combined Arms Combat
Developments Activity
Ft. Leavenworth, Kansas 66027

National Security Agency — 1 Copy
Ft. Geo. G. Meade, Maryland 20755
Attn: R. C. Foss A763

Deputy Commandant for Combat & Training Developments — 1 Copy
U. S. Army Ordnance Center and School
Attn: ATSL-CTD-MS-R
Aberdeen Proving Ground, Maryland 21005

Commanding Officer — 1 Copy
USACDC CBR Agency
Ft. McClellan, Alabama 36201
Attn: CDCCBR-MR (Mr. F. D. Poer)

Department of the Navy — 1 Copy
Office of the Chief of Naval Operations
Pentagon 5C739
Washington, D. C. 20350
Attn: (OP 982F3)

Office of Naval Research
Attn: Dr. Fred Quelle — 1 Copy
Dr. M. White — 1 Copy
495 Summer Street
Boston, Massachusetts 02210

Department of the Navy — 1 Copy
Deputy Chief of Naval Material (Dev.)
Washington, D. C. 20360
Attn: Mr. R. Gaylord (MAR 032B)

Naval Missile Center — 1 Copy
Point Mugu, California 93042
Attn: Gary Gibbs (Code 5352)

Naval Research Lab
Washington, D. C. 20375
Attn: (Code 5503-LTPO
Dr. P. Livingston (Code 55060) 1 Copy
Dr. A. I. Schindler (Code 6330) 1 Copy
Dr. H. Shenker (Code 6530) 1 Copy
Mr. D. J. McLaughlin (Code 5560) 1 Copy
Dr. John L. Walsh (Code 5503) 1 Copy

High Energy Laser Project Office 1 Copy
Department of the Navy
Naval Sea Systems Command
Washington, D. C. 20360
Attn: Capt. J. G. Wilson, USN (PMS-405)

Superintendent 1 Copy
Naval Postgraduate School
Monterey, California 93940
Attn: Library (Code 2124)

Navy Radiation Technology Liaison Office 1 Copy
Air Force Weapons Lab. (NLO)
Kirtland AFB, New Mexico 87117

Naval Surface Weapons Center
White Oak
Silver Spring, Maryland 20910
Attn: Dr. Leon H. Schindel (Code 310) 1 Copy
Dr. E. Leroy Harris (Code 313) 1 Copy
Mr. K. Enkenhus (Code 034) 1 Copy
Mr. J. Wise (Code 047) 1 Copy

U. S. Naval Weapons Center
China Lake, California 93555
Attn: (Code 5114) 1 Copy
Technical Library 1 Copy

HQ USAF (AF/RDPS) 1 Copy
Pentagon
Washington, D. C. 20330
Attn: Lt. Col. A. J. Chiota

HQ AFSC/XRLW 1 Copy
Andrews AFB
Washington, D. C. 20331
Attn: Mrj. J. M. Walton

HQ AFSC (DLCAW) — 1 Copy
Andrews AFB
Washington, D. C. 20331
Attn: Maj. H. Axelrod

Air Force Weapons Lab
Kirtland AFB, New Mexico 87117
Attn: LR — 4 Copies
AL — 2 Copies

HQ SAMSO (SRTD) — 1 Copy
P.O. Box 92960, Worldway Postal Center
Los Angeles, California 90009
Attn: Lt. Dorian DeMaio (XRTD)

AF Avionics Lab (TEO)
Wright Patterson AFB, Ohio 45433
Attn: Mr. K. Hutchinson — 1 Copy

Dept. of the Air Force
Air Force Materials Lab. (AFSC)
Wright Patterson AFB, Ohio 45433
Attn: Maj. Paul Elder (LPS) — 1 Copy
Laser Window Group

HQ Aeronautical Systems Division
Wright Patterson AFB, Ohio 45433
Attn: XRF - Mr. Clifford Fawcett — 1 Copy

Rome Air Development Command
Griffiss AFB
Rome, New York 13440
Attn: Mr. R. Urtz (OCSE) — 1 Copy

HQ Electronics Systems Div. (ESL)
L. G. Hanscom Field
Bedford, Massachusetts 01730
Attn: Mr. Alfred E. Anderson (XRT) — 1 Copy
Capt. James C. Jalbert (XRJ) — 1 Copy
Technical Library — 1 Copy

Air Force Rocket Propulsion Lab
Edwards AFB, California 93523
Attn: B. R. Bornhorst, (LKCG) — 1 Copy

Commander
U. S. Army Frankford Arsenal
Philadelphia, Pennsylvania 19137
Attn: Mr. M. Elnick SARFA-FCD
Bldg. 201-3
1 Copy

Air Force Aero Propulsion Lab
Wright Patterson AFB, Ohio 45433
Attn: Col. Walter Moe (CC)
1 Copy

Dept. of the Air Force
Foreign Technology Division
Wright Patterson AFB, Ohio 45433
Attn: PDTN
1 Copy

CINCSAC/INEP
Offutt AFB, Nebraska 68113
1 Copy

Commandant of the Marine Corps
Scientific Advisor (Code RD-1)
Washington, D. C. 20380
1 Copy

USAF/INAKA
Washington, D. C. 20330
Attn: Lt. Col. W. M. Truesdell
1 Copy

Aerospace Research Labs., (AP)
Wright Patterson AFB, Ohio 45433
Attn: Lt. Col. Max Duggins
1 Copy

Defense Intelligence Agency
Washington, D. C. 20301
Attn: Mr. Seymour Derler (DTIB)
1 Copy

Analytic Services, Inc.
5613 Leesbrug Pike
Falls Church, Virginia 22041
Attn: Dr. John Davis
1 Copy

Aerospace Corp.
P. O. Box 92957
Los Angeles, California 90009
Attn: Dr. G. P. Millburn
1 Copy

Massachusetts Institute of Technology
Lincoln Lab - P.O. Box 73
Lexington, Massachusetts 02173

Attn:	Dr. R. Kingston	1 Copy
	Dr. P. Ingwersen	1 Copy
	Dr. L. Tomasetta	1 Copy